IEEE Access
Multidisciplinary | Rapid Review | Open Access Journal

Received May 8, 2020, accepted May 20, 2020, date of publication May 25, 2020, date of current version June 5, 2020.

Digital Object Identifier 10.1109/ACCESS.2020.2997285

Improved User Fairness in Decode-Forward Relaying Non-Orthogonal Multiple Access Schemes With Imperfect SIC and CSI

FERDI KARA, (Member, IEEE), AND HAKAN KAYA
Wireless Communication Technologies Research Laboratory (WCTLab), Department of Electrical and Electronics Engineering, Zonguldak Bülent Ecevit University, 67100 Zonguldak, Turkey

Corresponding author: Ferdi Kara (f.kara@beun.edu.tr)

This work was supported by the Zonguldak Bülent Ecevit University under Grant 2019-75737790-01.

ABSTRACT Non-orthogonal multiple access (NOMA) is one of the key technologies to serve in ultra-dense networks with massive connections which is crucial for Internet of Things. Besides, NOMA provides better spectral efficiency compared to orthogonal multiple access. However, NOMA systems have been mostly investigated only in terms of ergodic capacity (EC) and outage probability (OP) whereas error performances have not been well-studied. In addition, in those analysis, mostly perfect successive interference canceler (SIC) is assumed or the considered imperfect SIC model is not reasonable. Besides, channel state information (CSI) errors are also not considered in most studies. However, this is not the case for the practical scenarios, and these imperfect SIC and CSI effects limit the performance of NOMA involved systems. Moreover, the imperfect SIC causes unfairness between users. In this paper, we introduce reversed decode-forward relaying NOMA (R-DFNOMA) to improve user fairness compared to conventional DFNOMA (C-DFNOMA). In the analysis, we define imperfect SIC effect as dependant to channel fading and with this imperfect SIC and CSI errors, we derive exact expressions of EC and OP. We also provide upper bound for EC, and asymptotic and lower bound expressions for OP. Furthermore, we evaluate bit error performance of the proposed R-DFNOMA and derive exact bit error probability (BEP) in closed-form with imperfect CSI which is the first study analyzing error performances of decode-forward relaying NOMA with imperfect CSI. Then, we define user fairness index in terms of all key performance indicators (KPIs) (i.e., EC, OP and BEP). Based on extensive simulations, all derived expressions are validated, and it is proved that the proposed R-DFNOMA provides better user fairness than C-DFNOMA in terms of all KPIs. Finally, we discuss the effect of power allocations at both source and relay on the performance metrics and user fairness.

INDEX TERMS NOMA, DF relaying, user fairness, power allocation, imperfect SIC, CSI errors, error analysis, outage, capacity.

I. INTRODUCTION

In recent years, exponential increase in connected devices (i.e., smart-phones, tablets, watches etc.) [1] to the internet and with the introduce of the Internet of Things (IoT), future radio networks (FRN) are keen to serve massive users in dense networks which is called Massive Machine Type Communication (mMTC) -one of the three major concepts of 5G and beyond- [2]. Non-orthogonal Multiple Access (NOMA) is seen as a strong candidate for mMTC in FRN due to its high spectral efficiency and ability to support massive connections [3]. In NOMA, users are assigned into same resource block to increase spectral efficiency and the most attracted scheme is power domain (PD)-NOMA where users share the same resource block with different power allocation coefficients [4]. The interference mitigation in PD-NOMA is held by successive interference canceler (SIC) [5]. Due to its potential for 5G and beyond, NOMA[1] has attracted tremendous attention from researchers where NOMA is widely investigated mostly in terms of achievable rate/ergodic

The associate editor coordinating the review of this manuscript and approving it for publication was Ahmed Mohamed Ahmed Almradi.

[1]NOMA is used for PD-NOMA after this point.

capacity (EC) and outage probability (OP) [6]. Besides, since only superposition coding at the transmitter and SICs at the receivers are required, the integration of NOMA with other physical layer techniques such as cooperative communication, mm-wave communication, multi-input-multi-output (MIMO) systems, visible light communication, etc. has also taken a remarkable attention [7].

A. RELATED WORKS AND MOTIVATION

One of the most attracted topics is the interplay between NOMA and cooperative communication which is held in three major concepts: 1) cooperative-NOMA [8], [9] where near users also act as relays for far user, 2) NOMA-based cooperative systems [10], [11] where NOMA is implemented to increase spectral efficiency of device-to-device communication and 3) relay-assisted/aided-NOMA where relays in the network help NOMA users to enhance coverage.

This paper focuses on the relay-assisted-NOMA networks. The relay-assisted-NOMA networks have also been analyzed widely in terms of various performance metrics such as EC, OP and energy efficiency. In these works, an amplify-forward (AF) or a decode-forward (DF) relay helps source/BS to transmit symbols to the NOMA users [12]. Hybrid DF/AF relaying strategy has been also proposed in [13] and the EC analysis is conducted. In case direct links from source to users are not available, tremendous studies have been devoted to investigating capacity and outage performances of relay-assisted NOMA networks with a half duplex AF/DF relay [14]–[16]. In [14]–[16], capacity and outage performances of users have been derived by assuming different fading channels (e.g., Rayleigh, Nakagami-m). Outage probability of half duplex relay-assisted-NOMA networks have also been analyzed when a direct link between the source and the users exists [17]. Then, a buffer-aided scheme has been proposed for relay-assisted-NOMA networks where merged symbols are transmitted instead of NOMA in the first phase (from source to relay) to increase spectral efficiency [18], [19]. Moreover, relay assisted-NOMA networks have been analyzed with partial channel state information (CSI) at transmitter [20], imperfect CSI at receiver [21], [22] and with hardware impairments [23] when a half duplex relay is located between the source and the users. There are also a few studies which investigate/analyze relay-assisted-NOMA networks with a full duplex relay in terms of capacity and outage probability [24]. Furthermore, relay selection schemes have been investigated when multiple relays are available [25]–[28]. Relay selection schemes are based on guaranteeing QoS of users and maximizing outage performances of users. In addition, two-way relaying strategies where relay operates as a coordinated multi-point (CoMP), have been investigated in terms of achievable rate and outage performance [29]–[32].

However, in aforementioned either conventional or relay-assisted NOMA networks, mostly perfect SIC is assumed. This is not a reasonable assumption when considered fading channels. To the best of the authors' knowledge, very limited studies investigate NOMA involved systems with imperfect SIC. In those works, the imperfect SIC effect is assumed to be independent from the channel fading coefficient as a Gaussian noise [23], [24], [30], [31], [33]. However, considering the subtraction process within SIC, the imperfect SIC effect cannot be assumed independent from the channel fading coefficient. Thus, this strict assumption should be relaxed and a more accurate/realistic imperfect SIC model should be defined. Moreover, once the imperfect SIC is taken into consideration, it is shown that in downlink NOMA schemes, users encounter a performance degradation in bit/symbol error rate (BER/SER) compared to orthogonal multiple access (OMA) though its performance gains in terms of EC and OP [34], [35]. Indeed, this performance degradation may be severe for one of the users. Hence, the user fairness should be also considered in system design when the users have similar channel conditions. Although the user fairness is raised in conventional downlink NOMA networks [36] and some studies are devoted to improving user fairness in conventional NOMA networks in terms of EC and OP [37]–[39], to the best of the authors' knowledge, there is no study in the literature which investigates user fairness in relay-assisted NOMA networks. The user unfairness becomes worse in relay-assisted-NOMA systems due to the effects of two phases (e.g., from source-to-relay and from relay-to-users).

In addition, although numerous studies have been devoted to analyzing NOMA networks in terms of EC and OP, very limited studies consider bit/symbol/block error rate (BER/SER/BLER) analysis and error performance of relay-assisted NOMA networks has been analyzed only in [40], [41]. However, the authors in [40], [41] consider that the perfect CSI is available at the relay and users and to the best of the authors' knowledge, error analysis of NOMA involved systems has not been conducted with imperfect CSI, yet. Besides, as discussed above, user fairness in NOMA networks has been analyzed only in terms of EC and OP whereas error performances has not been considered in even conventional NOMA networks though it is one of the most important key performance indicators (KPIs).

Based on above discussions, we introduce a reversed relay-assisted NOMA considering user fairness. The considered model has been analyzed in terms of all KPIs (e.g., EC, OP, BER) with a more accurate imperfect SIC model and imperfect CSI. The user fairness is also discussed for the considered model for all KPIs.

B. CONTRIBUTIONS

The main contributions of this paper are as follow:

- We introduce the reversed DF relaying NOMA (R-DFNOMA) to improve user fairness in conventional DFNOMA (C-DFNOMA).
- For a more accurate/realistic scenario, we re-define imperfect SIC effect as dependant to channel fading coefficient. The capacity and outage performances of the proposed R-DFNOMA are investigated with this imperfect SIC effect and CSI errors. The exact EC

TABLE 1. List of symbols, notations, and abbreviations.

P_i	Transmit power at node $i = s, r$
α_j	Power allocation at the source for user j
x_j	Modulated base-band (IQ) symbol of user j
$h_{i,k}$	Flat fading channel coefficient between nodes i and k
$\hat{h}_{i,k}$	Estimated channel for $h_{i,k}$
$\epsilon_{i,k}$	Estimation error
n_i	Additive white Gaussian noise (AWGN)
μ	Propagation constant
τ	Path loss exponent
$d_{i,k}$	Euclidean distance between i and k
$\sim$	Follows/distributed
$CN(m, \sigma^2)$	Complex Normal distribution with m mean and $\frac{\sigma^2}{2}$ variance in each component
$\|.\|$	Absolute value
ρ_i	Transmit signal-to-noise ratio (SNR)
$SINR_j^{i,k}$	Signal-to-interference plus noise ratio (SINR) for user j between nodes i and k
$\gamma_{i,k}$	Absolute square for channel fading between nodes i and k ($\|h_{i,k}\|^2$)
$\hat{x}_j$	Detected/estimated base-band (IQ) symbol of user j at relay
Ξ_i	Imperfect SIC effect coefficient at the node i
β_j	Power allocation at the relay for user j
$\tilde{x}_j$	Detected/estimated base-band (IQ) symbol of user j at destination
R_j	Achievable (Shannon) rate of user j
C_j	Ergodic capacity (EC) of user j
$f_Z(z)$	Probability density function (PDF) of random variable z
$F_Z(z)$	Cumulative distribution function (CDF) of random variable z
$\acute{R}_j$	Target rate of user j (QoS requirement)
$P_j(out)$	Outage probability (OP) of user j
$e2e$	End-to-end
$P_j^{(i,k)}(e)$	Bit error probability (BEP) of user j between nodes i and k
$P_j(e\|\gamma_{i,k})$	Conditional BEP on $\gamma_{i,k}$
$Q(.)$	Marcum-Q function $Q(z) = \int_z^\infty 1/\sqrt{2\pi} exp(-z^2/2) dz$
$\ni_{i,k}$	The noise terms at the receiver due to the CSI errors
$PF_l(out)$	Proportional fairness index $l = c, o, e$ $c \rightarrow$EC, $o \rightarrow$OP and $e \rightarrow$BEP

expressions are derived with imperfect SIC and CSI, then closed-form upper bounds are provided for EC for imperfect SIC and perfect CSI. Besides, the exact OP expressions are derived in closed-forms with imperfect SIC and CSI. Furthermore, asymptotic and lower bound (error floor) expressions are derived for OP in closed-forms with imperfect SIC and CSI. All derived expressions match perfectly with simulations.

- Contrary to the most of the literature, we also analyze error performance of the R-DFNOMA rather than only EC and/or OP performances. Firstly in the literature, the exact bit error probability (BEP) expressions with imperfect CSI are derived in closed-forms and validated via computer simulations. To this end, we reveal that the imperfect CSI effect in BEP analysis of NOMA schemes is quite different than the OMA schemes. The noise due to the imperfect CSI in BEP analysis is not always same and it has different variances according to transmitted superposition coded symbols of the users. The analysis is quite challenging since each possible of superposition coded symbols should be analyzed separately. Therefore, We reveal that the BEP analysis of NOMA involved systems with imperfect CSI should be further investigated.
- We evaluate performances of the proposed model in terms of all KPIs (i.e., EC, OP and BEP) and compared with the benchmark. In this content, to the best of the authors' knowledge, this is also the first study which provides an overall performance evaluation for any NOMA involved systems. All literature researches have biased on investigations for only one or two performance metrics (e.g., EC and/or OP).
- We define users fairness in terms of all KPIs (i.e., EC, OP and BEP). Based on extensive simulations, it is proved that the proposed R-DFNOMA provides better user fairness compared to C-DFNOMA. Finally, we reveal the effect of power allocation on user fairness and discuss optimum power allocation.

C. ORGANIZATION

The remainder of this paper is as follows. In Section II, the proposed R-DFNOMA and the benchmark C-DFNOMA schemes are introduced. The detection algorithms at the users and the signal-to-interference plus noise ratio (SINR) definitions are also provided in this section. Then, the performance analysis for three KPIs (i.e., EC, OP, BER) are derived in Section III and the user fairness indexes for all KPIs are provided. In Section IV, all derived expressions are validated via Monte Carlo simulations. In addition, performance comparisons are also revealed in this section. Finally, results are discussed and the paper is concluded in Section V.

D. NOTATION

The list of symbols, notations and abbreviations through this paper is given in Table 1.

II. SYSTEM AND CHANNEL MODEL

A. PROPOSED: REVERSED DF RELAYING IN NOMA

As shown in Fig. 1, a source (S) communicates with two destinations[2] (i.e., D_1 and D_2) with the help of a relay (R). The relay applies decode-forward (DF) strategy in a half-duplex

[2]Although more than two users can be implemented in NOMA, it is limited by two since increasing the number of users causes more inter-user-interference and users will have worse error performances. Thus, it is considered to be two users in also 3GPP standards [42].

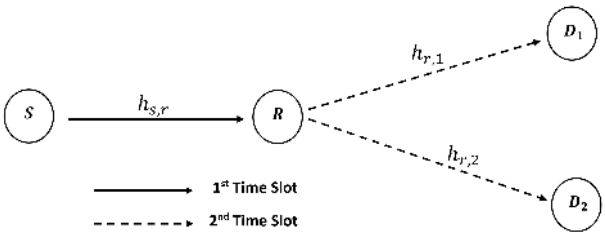

FIGURE 1. The illustration of R-DFNOMA.

mode, thus the total communication occupies two time slots. We assume that direct links from source to destinations are not available due to the high path-loss effects and/or obstacles. According to their average channel qualities[3] between relay and destinations (i.e., $R-D_1$ and $R-D_2$), users are defined as near and far users. We assume that D_1 has a better channel condition than D_2 to the relay node (R). In this case, D_1 and D_2 are denoted as the near and far users, respectively. The complex flat fading channel coefficient each node is represented by $h_{i,k}$ and follows $CN\left(0,\sigma_{i,k}^2\right)$ where $\{i,k\}\in[\{s,r\},\{r,1\},\{r,2\}]$. $\sigma_{i,k}^2$ includes the large-scale fading effects and $\sigma_{i,k}^2=\mu d_{i,k}^{-\tau}$ is defined where μ and τ are the propagation constant and path-loss exponent, respectively. $d_{i,k}$ is the Euclidean distance between the nodes. At the receiving nodes, channel state information (CSI) can not be known perfectly [22], thus the CSI (estimated channel) at each node is given by $\hat{h}_{i,k}$. $h_{i,k}=\hat{h}_{i,k}+\epsilon_{i,k}$ where $\epsilon_{i,k}$ follows $CN(0,\kappa_{i,k})$. Therefore, the $\hat{h}_{i,k}$ is dependant to $\epsilon_{i,k}$ and its variance is obtained by $\hat{\sigma}_{i,k}^2=\sigma_{i,k}^2-\kappa_{i,k}$. In the first phase of communication, the source (S) implements superposition coding for the base-band modulated symbols of the destinations (i.e., x_1 and x_2) and transmits it to the relay. The received signal by the relay is given as

$$y_{s,r}=\sqrt{P_s}\left(\hat{h}_{s,r}+\epsilon_{s,r}\right)\left(\sqrt{\alpha_1}x_1+\sqrt{\alpha_2}x_2\right)+n_r \quad (1)$$

where P_s is the transmit power of the source. n_r denotes the additive white Gaussian noise (AWGN) at the relay and follows $CN\,(0,N_0)$. In (1), α_1 and α_2 are the power allocation coefficients for the symbols of D_1 and D_2, respectively. In order to improve user fairness, in R-DFNOMA, we propose to allocate $\alpha_1>\alpha_2$ in the first phase where $\alpha_1+\alpha_2=1$. Unlike previous works, we propose to reverse power allocation coefficient in the first phase (i.e., $\alpha_1>\alpha_2$) and conventional power allocation is proposed in the second phase (i.e., $\beta_2>\beta_1$ -will be defined below-) whereas in conventional DFNOMA schemes, they have performed same way in both phases -as defined in benchmark in the next subsection. Thus, the proposed system model is called reversed-DFNOMA (R-DFNOMA). This reversed power allocation brings also reversed detecting order in the first phase. Since more power is allocated to D_1 symbols, the relay node (R) firstly detects x_1 symbols by pretending x_2 symbols as noise based on the received signal in the first phase. The maximum-likelihood (ML) detection of x_1 symbols at the relay is given

$$\hat{x}_1=\underset{k}{\operatorname{argmin}}\left|y_{s,r}-\sqrt{P_s}\hat{h}_{s,r}\sqrt{\alpha_1}x_{1,k}\right|^2 \quad (2)$$

where $x_{1,k}$ denotes the k th point in the M_1-ary constellation. The received signal-to-interference plus noise ratio (SINR) for the x_1 symbols at the relay is given by

$$SINR_1^{(s,r)}=\frac{\rho_s\alpha_1\hat{\gamma}_{s,r}}{\rho_s\alpha_2\hat{\gamma}_{s,r}+\kappa_{s,r}\rho_s+1} \quad (3)$$

where $\rho_s={}^{P_s}/_{N_0}$ and $\hat{\gamma}_{s,r}=\left|\hat{h}_{s,r}\right|^2$ are defined. The effect of imperfect CSI increases the exposed noise.

On the other hand, a successive interference canceler (SIC) should be implemented at the relay to detect less-powered x_2 symbols. The ML detection of x_2 symbols at the relay is given as

$$\hat{x}_2=\underset{k}{\operatorname{argmin}}\left|y'_{s,r}-\sqrt{P_s}\hat{h}_{s,r}\sqrt{\alpha_2}x_{2,k}\right|^2 \quad (4)$$

where

$$y'_{s,r}=y_{s,r}-\sqrt{P_s}\hat{h}_{s,r}\sqrt{\alpha_1}\hat{x}_1 \quad (5)$$

and $x_{2,k}$ denotes the k th point in the M_2-ary constellation. One can easily see that, the remaining signal after SIC highly depends on the detection of x_1 symbols and unlike previous works, it is not reasonable to assume perfect SIC (e.g., no interference from x_1 symbols). In addition, the interference after SIC is a function of $\hat{\gamma}_{s,r}$, P_s and α_1, due to the subtraction given in (5), thus the interference cannot be assumed an independent random variable unlike given in [24], [30], [31], [33] as independent Gaussian noise. To this end, the SINR for x_2 symbols at the relay is given as

$$SINR_2^{(s,r)}=\frac{\rho_s\alpha_2\hat{\gamma}_{s,r}}{\Xi_r\rho_s\alpha_1\hat{\gamma}_{s,r}+\kappa_{s,r}\rho_s+1} \quad (6)$$

where Ξ_r defines the imperfect SIC effect coefficient (e.g., $\Xi_r=0$ for perfect SIC and $\Xi_r=1$ for no SIC at all). The effect of imperfect CSI exists whether perfect or imperfect SIC is achieved.

In the second phase of communication, the relay node (R) again implements superposition coding for detected $\hat{x}_1$ and $\hat{x}_2$ symbols and broadcasts this total symbol to the destinations. The received signal by both destinations is given as

$$y_j=\sqrt{P_r}\left(\hat{h}_{r,j}+\epsilon_{r,j}\right)\left(\sqrt{\beta_1}\hat{x}_1+\sqrt{\beta_2}\hat{x}_2\right)+n_i \quad j=1,2 \quad (7)$$

where P_r is the transmit power of the relay.[4] n_i denotes the additive white Gaussian noise (AWGN) at the D_i and

[3]We assume that users are ordered according to statistical CSIT instead of instantaneous CSIT since ordering with instantaneous CSIT requires feedback signaling within each symbol duration and error free CSIT which is not reasonable. Thus, NOMA with statistical CSIT is more practical.

[4]The relay can harvest its energy from received RF signal to transmit signals [22], [43]. However, in this paper, this constraint has not been regarded and energy harvesting (EH) models such as linear and non-linear are seen as future researches.

$n_i \sim CN(0, N_0)$. We assume $d_{r,2} \geq d_{r,1}$, hence D_1 has better channel condition and more power allocated to D_2-user with weaker channel condition-, (i.e., $\beta_2 > \beta_1$ and $\beta_1 + \beta_2 = 1$). Based on the received signals, users implement whether ML or SIC plus ML in order to detect their own symbols. Since more power is allocated for the symbols of D_2, D_2 implements only ML by pretending D_1's symbols as noise and it is given,

$$\tilde{x}_2 = \underset{k}{\operatorname{argmin}} \left| y_{r,2} - \sqrt{P_2}\hat{h}_{r,2}\sqrt{\beta_2}x_{2,k} \right|^2. \tag{8}$$

The received SINR at the D_2 is given as

$$SINR_2^{(r,2)} = \frac{\rho_r \beta_2 \hat{\gamma}_{r,2}}{\rho_r \beta_1 \hat{\gamma}_{r,2} + \kappa_{r,2}\rho_r + 1}. \tag{9}$$

where $\rho_r = {}^{P_r}/_{N_0}$ is defined.

On the other hand, D_1 implements SIC in order to detect its own symbols. Thus, it firstly detects x_2 symbols and subtract regenerated forms from the received signal. The detection process at the D_1 is given as

$$\tilde{x}_1 = \underset{k}{\operatorname{argmin}} \left| y'_{r,1} - \sqrt{P_r}\hat{h}_{r,1}\sqrt{\beta_1}x_{1,k} \right|^2 \tag{10}$$

where

$$y'_{r,1} = y_{r,1} - \sqrt{P_r}\hat{h}_{r,1}\sqrt{\beta_2}\tilde{x}_2. \tag{11}$$

The received SINR after SIC at the D_1 is given as

$$SINR_1^{(r,1)} = \frac{\rho_r \beta_1 \hat{\gamma}_{r,1}}{\Xi_1 \rho_r \beta_2 \hat{\gamma}_{r,1} + \kappa_{r,1}\rho_r + 1} \tag{12}$$

where Ξ_1 defines the imperfect SIC effect coefficient at the D_1 likewise in relay. In (9) and (12), $\kappa_{r,i}\rho_r$, $i = 1, 2$ denotes the noise term due to the CSI error (i.e., $\epsilon_{r,i}$).

B. BENCHMARK: CONVENTIONAL DF RELAYING IN NOMA

In conventional DF relay-aided NOMA (C-DFNOMA) schemes, detecting order at both relay and user are the same. The power allocation in the first phase is arranged as $\alpha_2^* > \alpha_1^*$. Hence, the relay node (R) firstly detects x_2 symbols and implements SIC to detect x_1 symbols. To this end, given detection algorithms and SINR definitions eq. (2)-(6) should be re-defined. The detection of x_2 symbols at the relay is given

$$\hat{x}_2 = \underset{k}{\operatorname{argmin}} \left| y_{s,r} - \sqrt{P_s}\hat{h}_{s,r}\sqrt{\alpha_2^*}x_{2,k} \right|^2 \tag{13}$$

and of x_1 symbols

$$\hat{x}_1 = \underset{k}{\operatorname{argmin}} \left| y^+_{s,r} - \sqrt{P_s}\hat{h}_{s,r}\sqrt{\alpha_1^*}x_{1,k} \right|^2 \tag{14}$$

where

$$y^+_{s,r} = y_{s,r} - \sqrt{P_s}\hat{h}_{s,r}\sqrt{\alpha_2^*}\hat{x}_2. \tag{15}$$

The SINRs in the first phase of communication are given as

$$SINR_2^{(s,r)} = \frac{\rho_s \alpha_2^* \hat{\gamma}_{s,r}}{\rho_s \alpha_1^* \hat{\gamma}_{s,r} + \kappa_{s,r}\rho_s + 1} \tag{16}$$

and

$$SINR_1^{(s,r)} = \frac{\rho_s \alpha_1^* \hat{\gamma}_{s,r}}{\Xi_r \rho_s \alpha_2^* \hat{\gamma}_{s,r} + \kappa_{s,r}\rho_s + 1}. \tag{17}$$

The signal detections and the SINRs in the second phase of C-DFNOMA are the same in R-DFNOMA.

III. PERFORMANCE ANALYSIS

In this section, we analyze the proposed R-DFNOMA in terms of three KPIs (i.e., EC, OP and BEP) in order to evaluate its performance. Then, we define user fairness index for all three KPIs.

A. ERGODIC CAPACITY (EC)

Since the proposed model includes a relaying strategy, its achievable rate is limited by the weakest link. Hence, considering both $S - R$ and $R - D_1$ links, the achievable (Shannon) rate of D_1 is given as

$$R_1 = \frac{1}{2}\min\left\{\log_2\left(1 + SINR_1^{(s,r)}\right), \log_2\left(1 + SINR_1^{(r,1)}\right)\right\}. \tag{18}$$

where $\frac{1}{2}$ exists since the total communication covers two time slots. The ergodic capacity (EC) of D_1 is obtained by averaging R_1 over instantaneous SINRs in (3) and (12). It is given as

$$C_1 = \frac{1}{2}\int_0^\infty\int \log_2\left(1 + \min\left\{SINR_1^{(s,r)}, SINR_1^{(r,1)}\right\}\right) \times f_{\hat{\gamma}_{s,r}} f_{\hat{\gamma}_{r,1}} d\hat{\gamma}_{s,r} d\hat{\gamma}_{r,1} \tag{19}$$

where $f_{\hat{\gamma}_{s,r}}$ and $f_{\hat{\gamma}_{r,1}}$ are the probability density functions (PDFs) of $\hat{\gamma}_{s,r}$ and $\hat{\gamma}_{r,1}$, respectively. Let define $Z = \min\{X, Y\}$, the cumulative density function (CDF) of Z is given by $F_Z(z) = 1 - (1 - F_X(z))(1 - F_Y(z))$ where $F_X(.)$ and $F_Y(.)$ are the CDFs of X and Y, respectively [44]. Recalling, $\int_0^\infty \log_2(1+x) f_X(x) dx = \frac{1}{ln2}\int_0^\infty \frac{1-F_X(x)}{1+x} dx$ [45], with some algebraic manipulations, we derive EC of the D_1 as

$$C_1 = \frac{1}{2ln2}\int_0^\infty \frac{exp\left(-\frac{(1+\kappa_{s,r}\rho_s)z}{(\alpha_1 - \alpha_2 z)\rho_s \hat{\sigma}^2_{s,r}} - \frac{(1+\kappa_{r,1}\rho_s)z}{(\beta_1 - \beta_2 \Xi_1 z)\rho_r \hat{\sigma}^2_{r,1}}\right)}{1+z} dz \tag{20}$$

To the best of the authors' knowledge, (20) cannot be solved in closed-form analytically. Nevertheless, it can be easily computed by numerical tools. In addition, we can obtain upper bound in the closed-form for perfect CSI ($\kappa_{s,r} = \kappa_{r,1} = 0$) when assuming $\rho_s, \rho_r \to \infty$. In this case, $Z = \min\left\{SINR_1^{(s,r)}, SINR_1^{(r,1)}\right\}$ in (19) turns out to be $\lim_{\rho_s,\rho_r\to\infty} Z = min\left\{\frac{\alpha_1}{\alpha_2}, \frac{\beta_1}{\Xi_1\beta_2}\right\}$. With some algebraic simplifications, the upper bound for EC of the D_1 is given by

$$C_1^{(upper)} \approx \frac{1}{2}\log_2 \eta_1 \tag{21}$$

where $\eta_1 = min\left\{\frac{\alpha_1}{\alpha_2}, \frac{\beta_1}{\Xi_1\beta_2}\right\}$.

Likewise in capacity analysis of the D_1, the achievable rate of the D_2 is given by

$$R_2 = \frac{1}{2}\min\left\{\log_2\left(1+SINR_2^{(s,r)}\right), \log_2\left(1+SINR_2^{(r,2)}\right)\right\} \tag{22}$$

and taking the similar steps between (19)-(20), EC of the D_2 is derived as

$$C_2 = \frac{1}{2ln2}\int_0^{\infty} \frac{exp\left(-\frac{(1+\kappa_{s,r}\rho_s)z}{(\alpha_2-\alpha_1\Xi_r z)\rho_s\hat{\sigma}_{s,r}^2} - \frac{(1+\kappa_{r,2}\rho_r)z}{(\beta_2-\beta_1 z)\rho_r\hat{\sigma}_{r,2}^2}\right)}{1+z} dz. \tag{23}$$

Likewise (20), (21) can be easily computed by numerical tools. Again in order to obtain upper bound for perfect CSI ($\kappa_{s,r} = \kappa_{r,2} = 0$), if we assume $\rho_s, \rho_r \to \infty$, the EC is obtained as

$$C_2^{(upper)} \approx \frac{1}{2}\log_2 \eta_2 \tag{24}$$

where $\eta_2 = min\left\{\frac{\alpha_2}{\Xi_r\alpha_1}, \frac{\beta_2}{\beta_1}\right\}$.

B. OUTAGE PROBABILITY (OP)

The outage event for any user is defined as

$$P_j(out) = P\left(R_j < \acute{R}_j\right) \quad j = 1, 2 \tag{25}$$

where $\acute{R}_j$ is the target rate of D_j. By substituting (18) and (22) into (25), OPs of users are derived as

$$P_j(out) = P\left(\frac{1}{2}\min\left\{\log_2\left(1+SINR_j^{(s,r)}\right), \log_2\left(1+SINR_j^{(r,j)}\right)\right\} < \acute{R}_j\right) \quad j = 1, 2. \tag{26}$$

With some algebraic manipulations, OPs of users are derived as

$$P_j(out) = F_{Z_j}(\phi_j) \quad j = 1, 2 \tag{27}$$

where $\phi_j = 2^{2\acute{R}_j} - 1$ and $F_{Z_j}(.)$ CDF of $Z_j = \min\left\{SINR_j^{(s,r)}, SINR_j^{(r,j)}\right\}$ $j = 1, 2$ are defined. Recalling CDF for minimum of two exponential random variables in (20) and (23), OPs of users are derived in the closed-forms as in (28) and (29), as shown at the bottom of this page.

In the high SNR regime, we apply $e^{-x} \approx 1-x$ approximations [45] in (28) and (29), thus the high SNR approximations (asymptotic) for outage probabilities are derived as

$$P_1(out)^{(asymp)} \approx \begin{cases} \frac{(1+\kappa_{s,r}\rho_s)\phi_1}{(\alpha_1-\alpha_2\phi_1)\rho_s\hat{\sigma}_{s,r}^2} + \frac{(1+\kappa_{r,1}\rho_r)\phi_1}{(\beta_1-\beta_2\Xi_1\phi_1)\rho_r\hat{\sigma}_{r,1}^2}, \\ \quad \alpha_1 > \alpha_2\phi_1, \ \beta_1 > \beta_2\Xi_1\phi_1, \\ 1, \quad \text{otherwise}, \end{cases} \tag{30}$$

and

$$P_2(out)^{(asymp)} \approx \begin{cases} \frac{(1+\kappa_{s,r}\rho_s)\phi_2}{(\alpha_2-\alpha_1\Xi_r\phi_2)\rho_s\hat{\sigma}_{s,r}^2} + \frac{(1+\kappa_{r,2}\rho_r)\phi_2}{(\beta_2-\beta_1\phi_2)\rho_r\hat{\sigma}_{r,2}^2} \\ \quad \alpha_2 > \alpha_1\Xi_{s,r}\phi_2, \beta_2 > \beta_1\phi_2, \\ 1, \quad \text{otherwise}. \end{cases} \tag{31}$$

In addition, assuming $\rho_s, \rho_r \to \infty$, with some simplification, the lower bounds (error floor) with imperfect SIC and CSI are derived as

$$P_1(out)^{(lower)} = \begin{cases} \frac{\kappa_{s,r}\phi_1}{(\alpha_1-\alpha_2\phi_1)\hat{\sigma}_{s,r}^2} + \frac{\kappa_{r,1}\phi_1}{(\beta_1-\beta_2\Xi_1\phi_1)\hat{\sigma}_{r,1}^2}, \\ \quad \alpha_1 > \alpha_2\phi_1, \beta_1 > \beta_2\Xi_1\phi_1, \\ 1, \quad \text{otherwise}, \end{cases} \tag{32}$$

and

$$P_2(out)^{(lower)} = \begin{cases} \frac{\kappa_{s,r}\phi_2}{(\alpha_2-\alpha_1\Xi_r\phi_2)\hat{\sigma}_{s,r}^2} + \frac{\kappa_{r,2}\phi_2}{(\beta_2-\beta_1\phi_2)\hat{\sigma}_{r,2}^2} \\ \quad \alpha_2 > \alpha_1\Xi_{s,r}\phi_2, \beta_2 > \beta_1\phi_2, \\ 1, \quad \text{otherwise}. \end{cases} \tag{33}$$

C. BIT ERROR PROBABILITY (BEP)

Since a cooperative communication is included in the R-DFNOMA, the number of total erroneous bits from source to destination (i.e., end-to-end (e2e)) of users are given as

$$N_j = N_j\left(x_j \to \hat{x}_j\right) + N_j\left(\hat{x}_j \to \tilde{x}_j\right) - N_j\left(x_j \to \hat{x}_j\right) \cap N_j\left(\hat{x}_j \to \tilde{x}_j\right), \quad j = 1, 2 \tag{34}$$

where $N_j\left(x_j \to \hat{x}_j\right)$ and $N_j\left(\hat{x}_j \to \tilde{x}_j\right)$ denote the number of erroneous detected bits of D_j in the first and second phases,

$$P_1(out) = \begin{cases} 1 - exp\left(-\frac{(1+\kappa_{s,r}\rho_s)\phi_1}{(\alpha_1-\alpha_2\phi_1)\rho_s\hat{\sigma}_{s,r}^2} - \frac{(1+\kappa_{r,1}\rho_r)\phi_1}{(\beta_1-\beta_2\Xi_1\phi_1)\rho_r\hat{\sigma}_{r,1}^2}\right), & \alpha_1 > \alpha_2\phi_1, \ \beta_1 > \beta_2\Xi_1\phi_1, \\ 1, & \text{otherwise}, \end{cases} \tag{28}$$

$$P_2(out) = \begin{cases} 1 - exp\left(-\frac{(1+\kappa_{s,r}\rho_s)\phi_2}{(\alpha_2-\alpha_1\Xi_r\phi_2)\rho_s\hat{\sigma}_{s,r}^2} - \frac{(1+\kappa_{r,2}\rho_r)\phi_2}{(\beta_2-\beta_1\phi_2)\rho_r\hat{\sigma}_{r,2}^2}\right) & \alpha_2 > \alpha_1\Xi_{s,r}\phi_2, \ \beta_2 > \beta_1\phi_2, \\ 1, & \text{otherwise}. \end{cases} \tag{29}$$

respectively. If erroneous detections have been performed in both phase, this means that correct detection has been achieved from source to destinations (e2e). Thus, the set of intersection of erroneous detections (3rd term) is subtracted in (34). Considering all combinations, the BEPs of D_j are given as in (35), as shown at the bottom of this page.

Recalling that $N_j\left(x_j \to \hat{x}_j\right)$ and $N_j\left(\hat{x}_j \to \tilde{x}_j\right)$ events are statistically independent, thus with the law of total probability, BEPs of users are given as

$$P_j^{(e2e)}(e) = P_j^{(s,r)}(e)\left(1 - P_j^{(r,j)}(e)\right) + \left(1 - P_j^{(s,r)}(e)\right) P_j^{(r,j)}(e) \quad j = 1, 2 \tag{36}$$

where $P_j^{(s,r)}(e) = \frac{1}{M_j \log_2 M_j} \sum_{k=1}^{M_i} \sum_{\forall l \neq k} N_j\left(x_{j,k} \to \hat{x}_{j,l}\right)$ and $P_j^{(r,j)}(e) = \frac{1}{M_j \log_2 M_j} \sum_{l=1}^{M_j} \sum_{\forall p \neq l} N_j\left(\hat{x}_{j,l} \to \tilde{x}_{j,p}\right)$ denote the BEPs in the first and second phases, respectively. Thus, the BEPs in each phases should be firstly derived. Each phase of communication can be considered separately. In the first phase of communication, it turns out to be a conventional downlink NOMA system and the BEP of x_1 symbols will be the same with BEP of *far user* in downlink NOMA. Since the superposition is applied, the BEP of *far user* in NOMA is highly depended on the chosen constellation pairs (i.e., M_1 and M_2) [34], [35], [46]. Nevertheless, the conditional BEP on channel conditions (for perfect CSI) is given in the form, $P_j(e|_{\gamma_j}) = \sum_{q=1}^{L_j} \varsigma_{j,q} Q\left(\sqrt{2\nu_{j,q}\rho\gamma_j}\right)$ where L_j, $\varsigma_{j,q}$ and $\nu_{j,q}$ coefficients change according to chosen modulation constellation pairs for x_1 and x_2 symbols [47, Table 1]. However, in case of the imperfect CSI, since the interference/noise is increased with CSI errors, further analysis is required and it has not been derived in the literature, yet. Reformulating all BEP analysis of NOMA in case of $M_1 = M_2 = 4$, the conditional BEP of x_1 symbols in the first phase is given as

$$P_1^{(s,r)}(e|_{\hat{\gamma}_{s,r}}) = \frac{1}{4} \sum_{q=1}^{2} \sum_{p=1}^{2} Q\left(\sqrt{\frac{2\nu_q \rho_s \hat{\gamma}_{s,r}}{\zeta_{q,p}\kappa_{s,r}\rho_s + 1}}\right) \tag{37}$$

where $\nu_1 = \left(\sqrt{\alpha_1/2} - \sqrt{\alpha_2/2}\right)^2$ and $\nu_2 = \left(\sqrt{\alpha_1/2} + \sqrt{\alpha_2/2}\right)^2$. In (37), $\zeta_{q,1} = 1\ \forall q$ and $\zeta_{q,2} \triangleq 2\nu_q$ are defined for presentation simplicity. *Proof:* See Appendix A ■

Then, recalling $\hat{\gamma}_{s,r}$ is exponentially distributed, with the aid of [48], the average BEP (ABEP) of x_1 symbols in the first phase is obtained as,

$$P_1^{(s,r)}(e) = \frac{1}{8} \sum_{q=1}^{2} \sum_{p=1}^{2} \left(1 - \sqrt{\frac{\nu_q \rho_s \hat{\sigma}_{s,r}}{1 + \zeta_{q,p}\kappa_{s,r}\rho_s + \nu_q \rho_s \hat{\sigma}_{s,r}}}\right) \tag{38}$$

On the other hand, x_2 symbols in the first phase can be considered as *near user symbols* in conventional downlink NOMA, Thus, the conditional BEP should be derived considering correct and erroneous SIC cases. Considering the imperfect CSI, after summing these BEPs of two SIC cases, the conditional BEP of x_2 symbols in the first phase is derived as

$$P_2^{(s,r)}(e|_{\hat{\gamma}_{s,r}}) = \frac{1}{4} \sum_{q=1}^{5} (-1)^{(q+1)} \sum_{p=1}^{\lambda_q} \varsigma_{q,p} Q\left(\sqrt{\frac{2\nu_q \rho_s \hat{\gamma}_{s,r}}{\zeta_{q,p}\kappa_{s,r}\rho_s + 1}}\right) \tag{39}$$

where $\nu_3 = \frac{\alpha_2}{2}$, $\nu_4 = \left(2\sqrt{\alpha_1/2} - \sqrt{\alpha_2/2}\right)^2$ and $\nu_5 = \left(2\sqrt{\alpha_1/2} + \sqrt{\alpha_2/2}\right)^2$. In (35), $\lambda_3 = 3$ *otherwise* $\lambda_q = 2\ \forall q$, $\varsigma_{3,1} = 2$, otherwise $\varsigma_{q,p} = 1\ \forall q, p$, $\zeta_3 = [1, 2\nu_1, 2\nu_2]$, $\zeta_4 \triangleq \zeta_1$ and $\zeta_5 \triangleq \zeta_2$. *Proof:* See Appendix B. ■

By averaging over instantaneous $\hat{\gamma}_{s,r}$, the ABEP of x_2 symbols in the first phase is derived as

$$P_2^{(s,r)}(e) = \frac{1}{8} \sum_{q=1}^{5} (-1)^{(q+1)} \times \sum_{p=1}^{\lambda_q} \varsigma_{q,p} \left(1 - \sqrt{\frac{\nu_q \rho_s \hat{\sigma}_{s,r}}{1 + \zeta_{q,p}\kappa_{s,r}\rho_s + \nu_q \rho_s \hat{\sigma}_{s,r}}}\right) \tag{40}$$

In the second phase of communication, most of power is allocated to $\hat{x}_2$ symbols so that D_2 implements a ML detection without SIC, Hence, with the help of (37), the BEP of x_2 symbols in the second phase can be easily derived as

$$P_2^{(r,2)}(e|_{\hat{\gamma}_{r,2}}) = \frac{1}{4} \sum_{q=1}^{2} \sum_{p=1}^{2} Q\left(\sqrt{\frac{2\varphi_q \rho_r \hat{\gamma}_{r,2}}{\zeta_{q,p}\kappa_{r,2}\rho_r + 1}}\right) \tag{41}$$

where $\varphi_1 = \left(\sqrt{\beta_2/2} - \sqrt{\beta_1/2}\right)^2$ and $\nu_2 = \left(\sqrt{\beta_2/2} + \sqrt{\beta_1/2}\right)^2$. The same definitions below (37) are valid for $\zeta_{p,q}$ in terms of φ_q. By using (38), the ABEP is given as

$$P_2^{(r,2)}(e) = \frac{1}{8} \sum_{q=1}^{2} \sum_{p=1}^{2} \left(1 - \sqrt{\frac{\varphi_q \rho_r \hat{\sigma}_{r,2}}{1 + \zeta_{q,p}\kappa_{r,2}\rho_r + \nu_q \rho_r \hat{\sigma}_{r,2}}}\right) \tag{42}$$

Likewise, the BEP of x_1 symbols in the second phase can be easily obtained by repeating (39). The conditional BEP and the ABEP are given as

$$P_1^{(r,1)}(e|_{\hat{\gamma}_{r,1}}) = \frac{1}{4} \sum_{q=1}^{5} (-1)^{(q+1)} \sum_{p=1}^{\lambda_q} \varsigma_{q,p} Q\left(\sqrt{\frac{2\varphi_q \rho_r \hat{\gamma}_{r,1}}{\zeta_{q,p}\kappa_{r,1}\rho_r + 1}}\right) \tag{43}$$

$$P_j(e) = \frac{1}{M_j \log_2 M_j} \left[\sum_{k=1}^{M_j} \sum_{\forall l \neq k} \sum_{\forall p \neq l} N_j\left(x_{j,k} \to \hat{x}_{j,l}\right) + N_j\left(\hat{x}_{j,l} \to \tilde{x}_{j,p}\right) - N_j\left(x_{j,k} \to \hat{x}_{j,l}\right) \cap N_j\left(\hat{x}_{j,l} \to \tilde{x}_{j,p}\right)\right] \quad j = 1, 2 \tag{35}$$

and

$$P_1^{(r,1)}(e) = \frac{1}{8}\sum_{q=1}^{5}(-1)^{(q+1)} \times \sum_{p=1}^{\lambda_q} \varsigma_{q,p}\left(1-\sqrt{\frac{\varphi_q\rho_r\hat{\sigma}_{r,1}}{1+\zeta_{q,p}\kappa_{r,1}\rho_r+\varphi_q\rho_r\hat{\sigma}_{r,1}}}\right) \tag{44}$$

where $\varphi_3 = \frac{\beta_1}{2}$, $\varphi_4 = \left(2\sqrt{\beta_2/2}-\sqrt{\beta_1/2}\right)^2$ and $\varphi_5 = \left(2\sqrt{\beta_2/2}+\sqrt{\beta_1/2}\right)^2$. The same definitions for $\varsigma_{p,q}$, λ_q below (39) are valid in terms of φ_q in (43) and (44).

Lastly, substituting (38), (40), (42) and (44) into (36), the ABEPs of users are derived as in (45) and (46), as shown at the bottom of this page.

D. USER FAIRNESS

In this subsection, we define fairness between users' performances. In NOMA schemes, since the total power is allocated between users, the users have different performances. Due to the inter-user-interference and the SIC operation, one of the users may have better performance than the other. This performance gap can be higher in some performance metrics (e.g. EC and BER).

The performance gap between users should not be increased. We use proportional fairness (PF) index to compare users' performances for all KPIs. For instance, let we firstly consider EC. In this case, if the fairness has not been considered, one of the users may achieve much more EC than the other. To alleviate this unfair situation, PF index for EC should be defined and it is given as

$$PF_c = \frac{C_1}{C_2} \tag{47}$$

which can be easily obtained by substituting (20) and (23) into (47). One can easily see that the optimum value for PF_c can be considered as 1 which means that both user have exactly the same EC. Nevertheless, this may not be achieved when the users have different QoS requirements. Thus, fairness indexes should be obtained for other KPIs and all three should be evaluated together. To this end, fairness indexes for outage and error performances are given as

$$PF_o = \frac{P_1(out)}{P_2(out)} \tag{48}$$

and

$$PF_e = \frac{P_1(e)}{P_2(e)} \tag{49}$$

which can be computed by substituting (28), (29) into (48) and (45), (46) into (49), respectively. It is again clear that the optimal values for PF_o and PF_e are also 1. However likewise in PF_c, it may not be always achieved due to the priority in QoS requirements of users. It is noteworthy that in the PF index for all KPIs, χ and $1/\chi$ have the same meaning. For instance, if the PF index for any performance metric has 2 and/or 0.5, this means that one of the users has two times better performance than the other.

IV. PERFORMANCE EVALUATION

In this section, we provide validation of the provided analysis in the previous sections. In addition, we present user fairness comparisons between the proposed R-DFNOMA and C-DFNOMA.[5] In all simulations, the transmit powers of source and relay are assumed to be equal (i.e., $P_s = P_r$). In validations of the R-DFNOMA, unless otherwise stated, curves denote theoretical analysis[6] and simulations are demonstrated by markers. Moreover, in all

[5]In C-DFNOMA, power allocation in the first phase is complement of the power allocation of R-DFNOMA (i.e., $\alpha_1^* = 1-\alpha_1$)

[6]In numerical integration for exact EC, the infinity in the upper bounds of the integrals is changed with 10^3 not to cause numerical calculation errors.

$$\begin{aligned} P_1^{(e2e)}(e) &= \frac{1}{8}\sum_{q=1}^{2}\sum_{p=1}^{2}\left(1-\sqrt{\frac{\nu_q\rho_s\hat{\sigma}_{s,r}}{1+\zeta_{q,p}\kappa_{s,r}\rho_s+\nu_q\rho_s\hat{\sigma}_{s,r}}}\right)\times\left[1-\frac{1}{8}\sum_{q=1}^{5}(-1)^{(q+1)}\sum_{p=1}^{\lambda_q}\varsigma_{q,p}\left(1-\sqrt{\frac{\varphi_q\rho_r\hat{\sigma}_{r,1}}{1+\zeta_{q,p}\kappa_{r,1}\rho_r+\varphi_q\rho_r\hat{\sigma}_{r,1}}}\right)\right] \\ &+\left[1-\frac{1}{8}\sum_{q=1}^{2}\sum_{p=1}^{2}\left(1-\sqrt{\frac{\nu_q\rho_s\hat{\sigma}_{s,r}}{1+\zeta_{q,p}\kappa_{s,r}\rho_s+\nu_q\rho_s\hat{\sigma}_{s,r}}}\right)\right]\times\frac{1}{8}\sum_{q=1}^{5}(-1)^{(q+1)}\sum_{p=1}^{\lambda_q}\varsigma_{q,p}\left(1-\sqrt{\frac{\varphi_q\rho_r\hat{\sigma}_{r,1}}{1+\zeta_{q,p}\kappa_{r,1}\rho_r+\varphi_q\rho_r\hat{\sigma}_{r,1}}}\right) \end{aligned} \tag{45}$$

$$\begin{aligned} P_2^{(e2e)}(e) &= \frac{1}{8}\sum_{q=1}^{2}(-1)^{(q+1)}\sum_{p=1}^{\lambda_q}\varsigma_{q,p}\left(1-\sqrt{\frac{\nu_q\rho_s\hat{\sigma}_{s,r}}{1+\zeta_{q,p}\kappa_{s,r}\rho_s+\nu_q\rho_s\hat{\sigma}_{s,r}}}\right)\times\left[1-\frac{1}{8}\sum_{q=1}^{2}\sum_{p=1}^{2}\left(1-\sqrt{\frac{\varphi_q\rho_r\hat{\sigma}_{r,2}}{1+\zeta_{q,p}\kappa_{r,2}\rho_r+\nu_q\rho_r\hat{\sigma}_{r,2}}}\right)\right] \\ &+\left[1-\frac{1}{8}\sum_{q=1}^{2}(-1)^{(q+1)}\sum_{p=1}^{\lambda_q}\varsigma_{q,p}\left(1-\sqrt{\frac{\nu_q\rho_s\hat{\sigma}_{s,r}}{1+\zeta_{q,p}\kappa_{s,r}\rho_s+\nu_q\rho_s\hat{\sigma}_{s,r}}}\right)\right]\times\frac{1}{8}\sum_{q=1}^{2}\sum_{p=1}^{2}\left(1-\sqrt{\frac{\varphi_q\rho_r\hat{\sigma}_{r,2}}{1+\zeta_{q,p}\kappa_{r,2}\rho_r+\nu_q\rho_r\hat{\sigma}_{r,2}}}\right) \end{aligned} \tag{46}$$

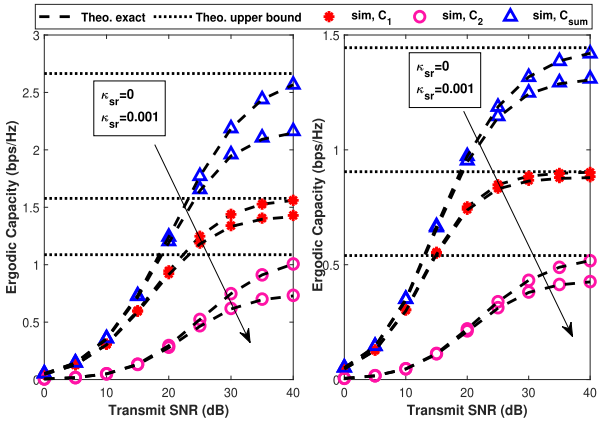

FIGURE 2. EC of R-DFNOMA vs ρ_S when $\alpha_1 = 0.9$, $\beta_1 = 0.2$, $d_{s,r} = 5$, $d_{r,1} = 1$ and $d_{r,2} = 3$ a) $\Xi_r = -15dB$ b) $\Xi_r = -10dB$.

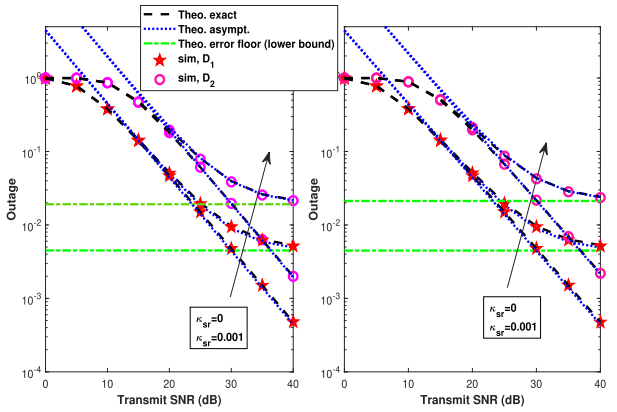

FIGURE 3. OP of R-DFNOMA vs ρ_S when $\alpha_1 = 0.9$, $\beta_1 = 0.2$,$\acute{R}_1 = 0.2$ and $\acute{R}_2 = 0.1$ a) $\Xi_r = -15dB$ b) $\Xi_r = -10dB$.

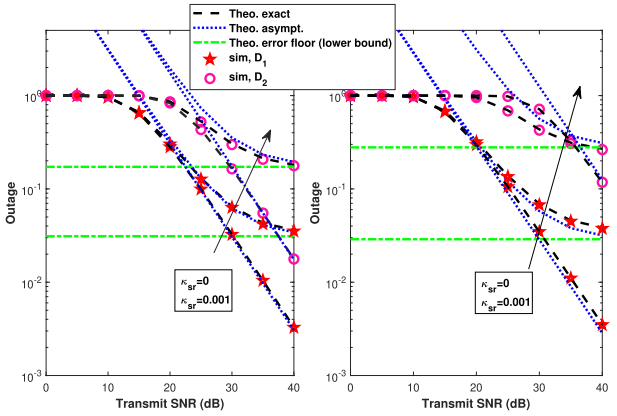

FIGURE 4. OP of R-DFNOMA vs ρ_S when $\alpha_1 = 0.9$, $\beta_1 = 0.2$, $\acute{R}_1 = 0.75$ and $\acute{R}_2 = 0.5$, a) $\Xi_r = -15dB$ b) $\Xi_r = -10dB$.

simulations, the imperfect SIC effect coefficients at the both nodes (i.e., $\Xi_r = \Xi_1$) and the variances of the channel estimation errors in all nodes are assumed to be equal (i.e., $\kappa_{s,r} = \kappa_{r,1} = \kappa_{r,2}$).

A. THE EFFECTS OF IMPERFECT SIC AND CSI

In this subsection, we assume that $\mu = 10$ and $\tau = 3$. The distances between the nodes are assumed to be $d_{s,r} = 5$, $d_{r,1} = 1$ and $d_{r,2} = 3$. It can be seen from following figures that all derived exact expressions match perfectly with simulations.

In Fig. 2, EC of the users and ergodic sum-rate of the R-DFNOMA ($C_{sum} = C_1 + C_2$) are given for various imperfect SIC ($\Xi_r = -15dB$ and $\Xi_r = -10dB$) and CSI ($\kappa_{s,r} = 0$ (perfect CSI) and $\kappa_{s,r} = 0.001$) effects. Power allocations are assumed to be $\alpha_1 = 0.9$, $\beta_1 = 0.2$. In addition to perfect math of exact expressions, provided upper bounds are also tight for perfect CSI. As it is expected, when the perfect CSI is not available at the receivers, the ECs of users get worse and this decay becomes more in high SNR regime. Besides, the imperfect SIC also limits the performance of the systems and when it gets higher (i.e., $\Xi_r = \Xi_1 = -10dB$), EC of the R-DFNOMA becomes worse. The power allocations at the source and relay are chosen as different values for better illustration, otherwise both users' upper bound would be the same.

In Fig. 3 and Fig. 4, outage performances of the users are presented for two different QoS requirements as $\acute{R}_1 = 0.2$, $\acute{R}_2 = 0.1$ and $\acute{R}_1 = 0.75$, $\acute{R}_2 = 0.5$, respectively. The same power allocation coefficients, the imperfect SIC effects and CSI errors are assumed as in Fig. 2. It can be seen that provided asymptotic and lower bound (error floor) expressions match well with simulations in addition to perfect match of exact expressions. In all NOMA involved systems, the outage performances of the users get better with low QoS requirements (e.g., lower target rates (Fig.3)). Likewise, in EC performance, with the CSI errors, a decay in outage performances occurs and an error floor in the high SNR regime exists. Besides, the imperfect SIC also affects the outage performances of users. This effect may be similar with lower QoS requirements (see Fig. 3.a and Fig. 3.b), however, with higher QoS requirements, its effect becomes severe and it may cause users to be in outage (see Fig.4.a and Fig. 4.b).

In order to further investigate the effect of imperfect SIC, we present capacity and outage performance of users with the change of imperfect SIC effect coefficient in Fig. 5 and Fig. 6, respectively. The power allocation coefficients at the source and the relay are assumed to be $\alpha_1 = 0.8$, $\beta_1 = 0.2$ and $\alpha_1 = 0.9$, $\beta_1 = 0.1$. The result are presented for $\rho_s = 30dB$ and $\kappa_{s,r} = 0.001$. The outage results are presented for three QoS requirements where $\acute{R}_1 = 0.2$, $\acute{R}_2 = 0.1$ in *QoS-I*, $\acute{R}_1 = 0.75$, $\acute{R}_2 = 0.5$ in *QoS-II* and $\acute{R}_1 = 1$, $\acute{R}_2 = 0.75$ in *QoS-III*. In both figures, as expected, with the increase of imperfect SIC effect, users have worse performance in both EC and OP. In Fig. 5, the system will have almost 0.5 capacity if the imperfect SIC effect is higher than $-5dB$ that is too poor performance for $30dB$ SNR. In Fig. 6, for the same imperfect SIC conditions, users are always in outage for all target rates. Indeed, if more strict QoS requirements are needed (higher

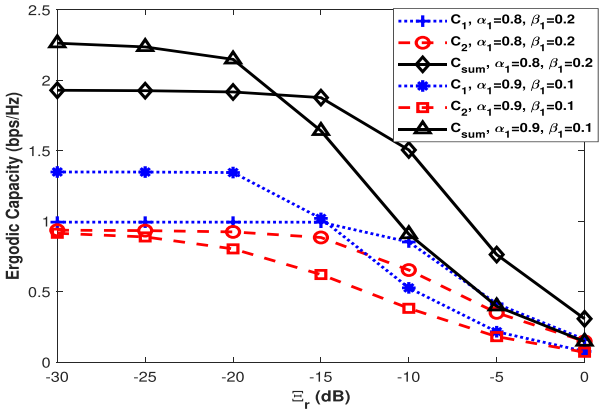

FIGURE 5. The effect of imperfect SIC on EC of R-DFNOMA when $d_{s,r} = 5$, $d_{r,1} = 1$, $d_{r,2} = 3$, $\rho_s = 30dB$ and $\kappa_{s,r} = 0.001$.

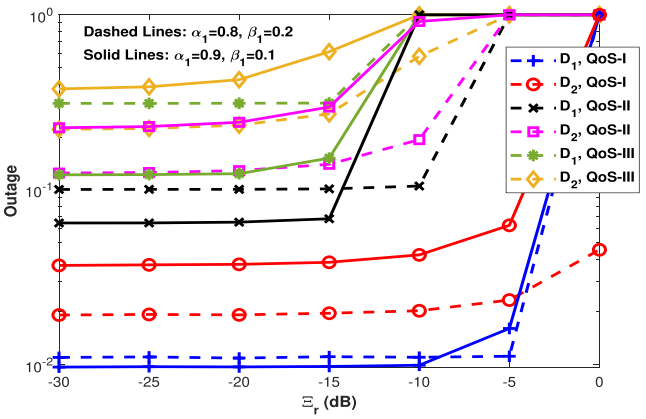

FIGURE 6. The effect of imperfect SIC on outage of R-DFNOMA when $d_{s,r} = 5$, $d_{r,1} = 1$, $d_{r,2} = 3$, $\rho_s = 30dB$ and $\kappa_{s,r} = 0.001$.

target rates), users will be in outage even for lower imperfect SIC effects (e.g., between $-10dB$ and $-5dB$). Nevertheless, all these are expected results for imperfect SIC case and represent more practical/reasonable scenarios than perfect SIC.

In Fig. 7, we present error performances of users in R-DFNOMA. In error performance simulations, since an actual modulation/demodulation (i.e., QPSK for $M_i = 4$) is implemented contrary to EC and OP simulations, imperfect SIC effect coefficient has not been defined. The erroneous detected symbols during SIC process will show this effect. Thus, we present simulations for two different power allocation pairs (i.e., $\alpha_1 = 0.8$, $\beta_1 = 0.2$ and $\alpha_1 = 0.9$, $\beta_1 = 0.1$). The CSI errors are presented for two cases, i.e., $\kappa_{s,r} = 0$ (perfect CSI) and $\kappa_{s,r} = 0.001$. Just as in previous validations, it is clearly seen in Fig. 7 that derived expressions are perfectly-matched with simulations. Besides, the imperfect CSI also limits the error performance of users and may cause an error floor in high SNR region.

B. USER FAIRNESS

Contrary to commonly belief, NOMA users do not need to have different channel conditions (stronger and weaker). NOMA users can be chosen among users with similar channel conditions [49], [50]. In this case, user fairness turns out to be more important, since none of them should be served with lower KPI. Thus, user fairness comparisons are more meaningful when the users experience similar channel conditions. To this end, we provide PF index comparisons between R-DFNOMA and C-DFNOMA in Fig. 8- Fig. 10 when $d_{s,r} = 5$ and $d_{r,1} = d_{r,2} = 2$. We assume that $\mu = 10$, $\tau = 2$ and for the imperfect CSI $\kappa_{s,r} = 0.001$. As seen from above figures, imperfect CSI affects both user in the same manner, thus with the change of imperfect CSI, proportional fairness indexes remain unchanged. In comparisons, two different power allocations scenarios are set $\alpha_1 = 0.9$, $\beta_1 = 0.1$ and $\alpha_1 = 0.8$, $\beta_1 = 0.2$, respectively. In Fig. 8 and Fig. 9, the imperfect SIC effect coefficients are set $\Xi_r = -10dB$ and $\Xi_r = -15dB$. Since the users have similar channel conditions, their target rates are chosen as $\acute{R}_1 = \acute{R}_2 = 0.5$ for PF_o. One can easily see that the proposed R-DFNOMA provides better user fairness than C-DFNOMA in terms of all KPIs. In proposed R-DFNOMA, users' performance orders are also reversed. In terms of EC in Fig. 8, D_1 has higher EC than D_2 in R-DFNOMA, hence the fairness index is higher than 1 whereas it is vice-versa in C-DFNOMA. Nevertheless, R-DFNOMA outperforms C-DFNOMA considering user fairness. For instance, when $\alpha_1 = 0.9$, $\beta_1 = 0.1$ and $\Xi_r = -10dB$, $PF_c = 1.545$ at $15dB$ SNR in R-DFNOMA which means D_1 has 1.545 times better EC than D_2 at $15dB$. However, for the same conditions, $PF_c = 0.2433$ in C-DFNOMA, which means D_2 has 4.11 times better EC than D_1.[7] In addition, it is obvious that R-DFNOMA provides optimum user fairness in high SNR regimes ($PF_c \to 1$) whereas it cannot be achieved in C-DFNOMA. Once user fairness is considered in terms of outage performance, the improvement by the proposed R-DFNOMA becomes outstanding in Fig. 9. In all considered scenarios, R-DFNOMA achieves about $PF_o = 0.5$ for all SNR region which means D_1 has 2 times better OP than D_2. However, in C-DFNOMA, with the increase of transmit SNR, user unfairness gets worse. Indeed, in some scenarios user fairness becomes atrocious with the increase of SNR. For instance, when $\alpha_1 = 0.9$, $\beta_1 = 0.1$ and $\Xi_r = -10dB$, $PF_o \to 80$ at $SNR \to 40dB$ which means D_2 has 80 times better OP than D_1 although they have same channel conditions. Likewise user fairness comparisons for EC and OP, the proposed R-DFNOMA is superior to C-DFNOMA also in terms of error performance in Fig. 10. Furthermore, this improvement is significant in some scenarios. For instance, when $\alpha_1 = 0.9$, $\beta_1 = 0.1$, with the increase of SNR ($\rho_s \to 40dB$), $PF_e \to 2$ in R-DFNOMA whereas $PF_e \to 7$ in C-DFNOMA which is a superb gain for data reliability of D_2.

[7] As discussed in the previous sections, we hereby again note that PF index of any performance metrics have the same meaning for χ and $1/\chi$. It only defines which user has better performance.

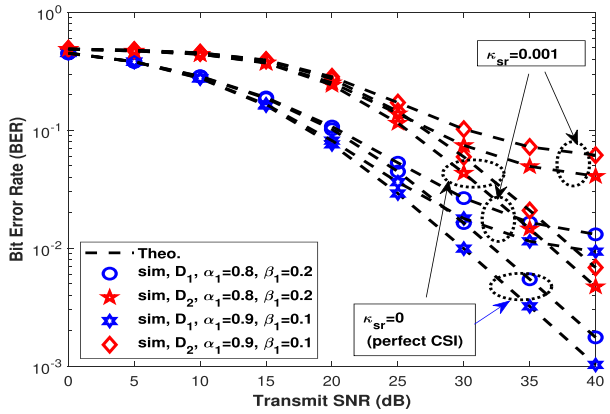

FIGURE 7. BER of R-DFNOMA vs ρ_S when $d_{s,r} = 5$, $d_{r,1} = 1$ and $d_{r,2} = 3$.

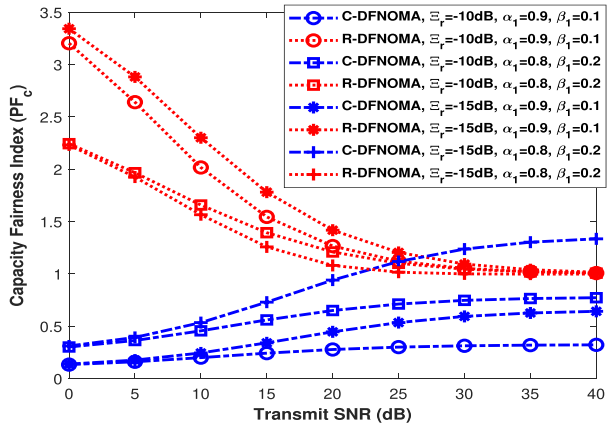

FIGURE 8. Capacity Fairness Index (PF_C) vs ρ_S when $d_{s,r} = 5$ and $d_{r,1} = d_{r,2} = 2$.

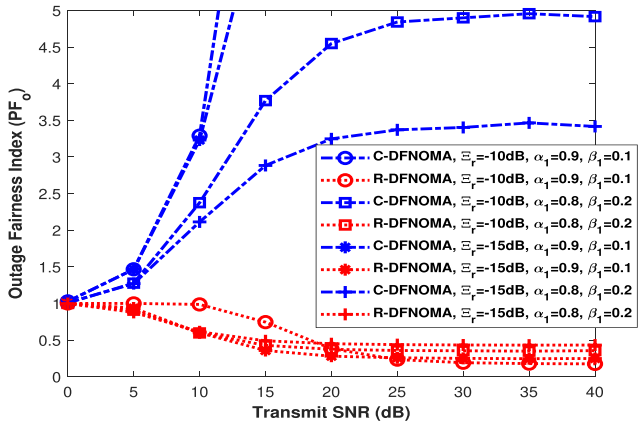

FIGURE 9. Outage Fairness Index (PF_O) vs ρ_S when $d_{s,r} = 5$, $d_{r,1} = d_{r,2} = 2$ and $\acute{R}_1 = \acute{R}_2 = 0.5$.

If the comparisons between C-DFNOMA and proposed R-DFNOMA are studied only in terms of fairness indexes (e.g., Fig. 8- Fig. 10), the questions may be raised that: Are the user fairness indexes be improved by degrading both of users' performances? or does the R-DFNOMA has worse performance? In order to resolve this concern and to prove

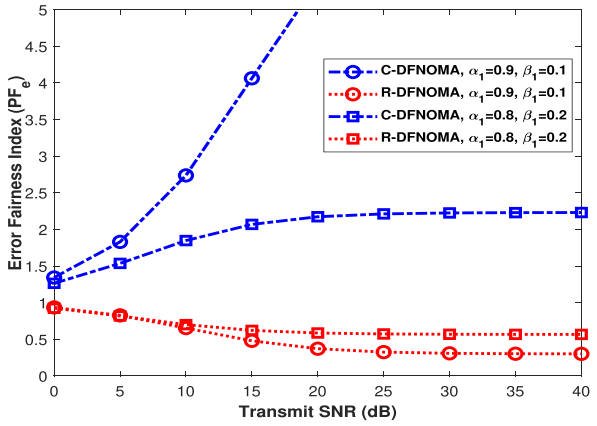

FIGURE 10. Error Fairness Index (PF_e) vs ρ_S when $d_{s,r} = 5$ and $d_{r,1} = d_{r,2} = 2$.

that R-DFNOMA achieves better user fairness indexes without degrading users' individual and overall performances, we present performance comparison between C-DFNOMA and R-DFNOMA in Fig. 11. The channel conditions are assumed to be the same with above comparisons and the power allocations are fixed as $\alpha_1 = 0.8$, $\beta_1 = 0.2$. The results are presented for both $\kappa_{s_r} = 0$ (perfect CSI) and $\kappa_{s_r} = 0.001$. In capacity and outage comparisons in Fig. 11.a and Fig. 11.b, the imperfect SIC effect coefficient is $\Xi_r = -15dB$ and the target rates of users are $\acute{R}_1 = \acute{R}_2 = 0.5$. As can be easily from Fig. 11 that in R-DFNOMA, users performances for all KPIs (i.e., EC, OP and BEP) get closer so that user fairness indexes are improved. Besides, when this improvement is achieved, the proposed R-DFNOMA does not cause performance decay in either users' or in overall system performances. When the users have similar channel conditions, the overall system performance is limited by the minimum performance achieved within users. To this end, in order to evaluate both systems (e.g., C-DFNOMA and R-DFNOMA), we can define performance metrics as

$$\begin{aligned} C^{(m)} &= \min\{C_1, C_2\}, \ m : C - DFNOMA \ or \ R - DFNOMA \\ P^{(m)}(out) &= \max\{P_1(out), P_2(out)\}, \\ P^{(m)}(e) &= \max\{P_1(e), P_2(e)\}. \end{aligned} \tag{50}$$

and the performance comparisons between R-DFNOMA and C-DFNOMA are given by

$$\begin{aligned} &\max\left\{C^{(C-DFNOMA)}, C^{(R-DFNOMA)}\right\}, \\ &\min\left\{P^{(C-DFNOMA)}(out), P^{(R-DFNOMA)}(out)\right\}, \\ &\min\left\{P^{(C-DFNOMA)}(e), P^{(R-DFNOMA)}(e)\right\}. \end{aligned} \tag{51}$$

Considering performance comparisons in (50)-(51), we can see from Fig. 11 that, C-DFNOMA and R-DFNOMA have the same performances in terms of theoretical Shannon rate (e.g., Fig. 11.a) where the minimums of users' rates are the same in C-DFNOMA and R-DFNOMA. Although it

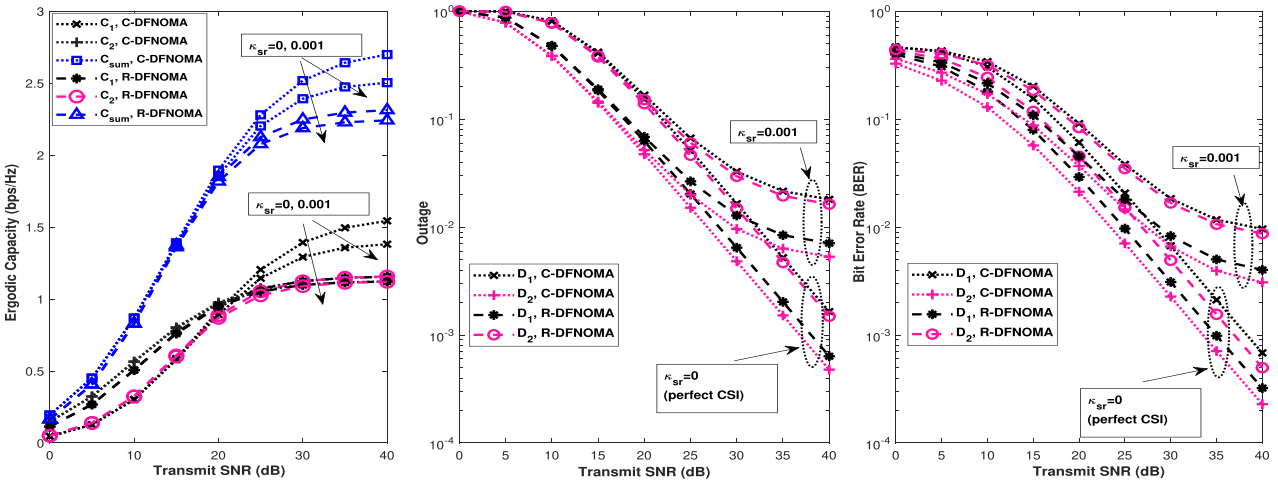

FIGURE 11. Performance comparisons between C-DFNOMA and R-DFNOMA vs ρ_S when $d_{s,r} = 5$, $d_{r,1} = d_{r,2} = 2$, $\alpha_1 = 0.8$ and $\beta_1 = 0.2$ a) Capacity when $\Xi_r = -15dB$ b) Outage when $\Xi_r = -15dB$ and $\acute{R}_1 = \acute{R}_2 = 0.5$ c) bit error rate.

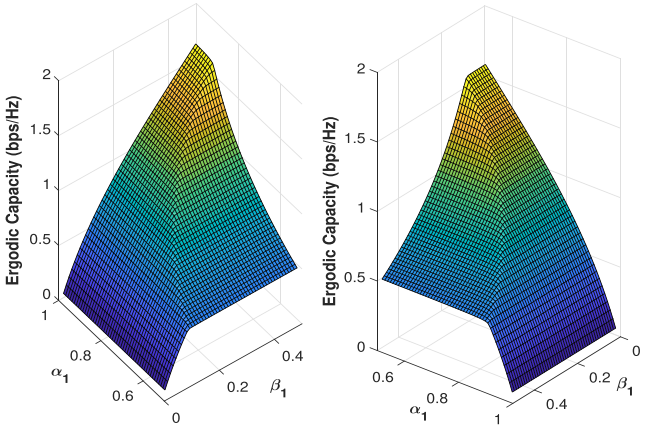

FIGURE 12. EC performance in R-DFNOMA vs α_1 and β_1 when $d_{s,r} = 5$, $d_{r,1} = d_{r,2} = 2$, $\rho_S = 30dB$ and $\Xi_r = -10dB$ a) D_1 b) D_2.

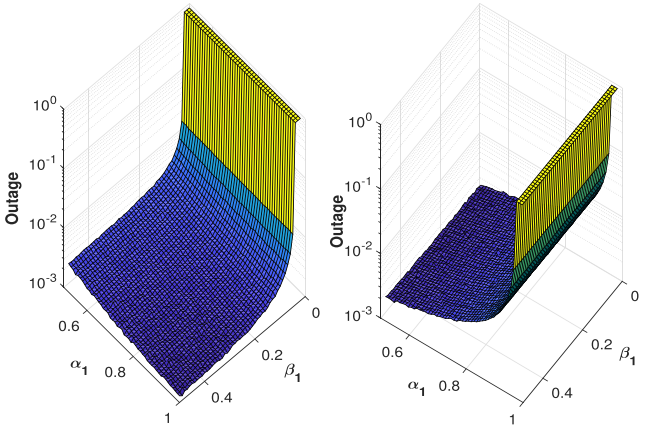

FIGURE 13. Outage performance in R-DFNOMA vs α_1 and β_1 when $d_{s,r} = 5$, $d_{r,1} = d_{r,2} = 2$, $\rho_S = 30dB$, $\Xi_r = -10dB$ and $\acute{R}_1 = \acute{R}_2 = 0.2$ a) D_1 b) D_2.

seems that D_1 in C-DFNOMA may have higher achievable rate in high SNR region, this should be jointly evaluated with performance of SIC receivers. It is proved in [46] that when the higher modulation orders (mean higher achievable rate) are implemented, none of the users' symbols cannot be detected and all users have 0.5 BER performance. On the other hand, the R-DFNOMA outperforms C-DFNOMA in terms of outage and BER performances. In Fig. 11.b, D_2 has the maximum outage probability in R-DFNOMA (performance limit as given in (50)) whereas D_1 has the maximum in C-DFNOMA and D_2 in R-DFNOMA has lower OP (better performance as given in (51)) than D_1 in C-DFNOMA. Once the same evaluations have been discussed for BER performances, we can easily see that D_2 in R-DFNOMA (maximum in R-DFNOMA) has lower BER (better performance as given in (51)) than D_1 in C-DFNOMA (maximum in C-DFNOMA). Besides, above discussions are valid for both perfect and imperfect CSI case. In other words, the R-DFNOMA is robust against CSI errors according to (50) and (51).

C. THE EFFECT OF POWER ALLOCATIONS

From above simulations and discussions, it can be seen that power allocations at the both nodes (source and relay) have a remarkable effect on the performance of the R-DFNOMA so that on the user fairness. Thus, in order to reveal this effect, we present EC, OP and BER performances of users with respect to power allocations (α_1 and β_1) in Fig. 12 - Fig. 14. The channel conditions are assumed to be $d_{s,r} = 5$, $d_{r,1} = d_{r,2} = 2$, $\mu = 10$ and $\tau = 2$. The imperfect SIC effect is $\Xi_r = -10dB$ assumed in EC and OP comparisons and transmit SNR $\rho_s = 30dB$ is assumed in all figures. Target rates of users are assumed to be equal to $\acute{R}_1 = \acute{R}_2 = 0.2$. The effect of power allocation can be also evaluated with different imperfect CSI effects. Nevertheless, it is proved that the imperfect CSI affects both users in same way/ratio. Thus, no to make

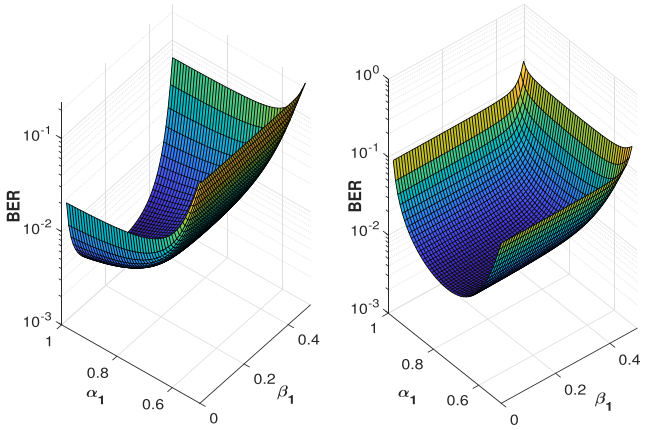

FIGURE 14. BER performance in R-DFNOMA vs α_1 and β_1 when $d_{s,r} = 5$, $d_{r,1} = d_{r,2} = 2$, $\rho_S = 30dB$ a) D_1 b) D_2.

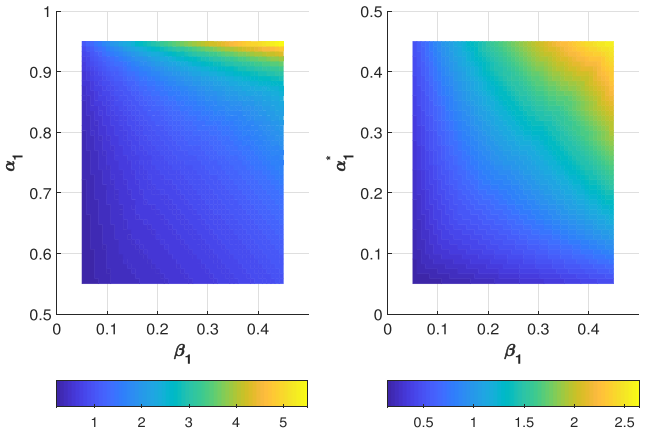

FIGURE 15. Capacity Fairness Index (PF_C) vs α_1 and β_1 when $d_{s,r} = 5$, $d_{r,1} = d_{r,2} = 2$, $\rho_S = 30dB$ and $\Xi_r = -10dB$ a) R-DFNOMA b) C-DFNOMA.

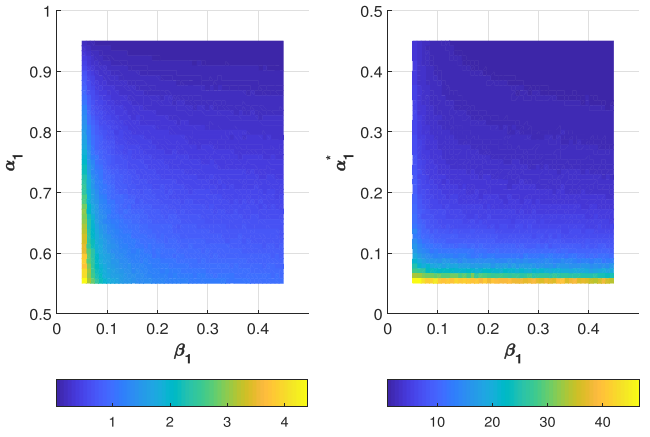

FIGURE 16. Outage Fairness Index (PF_O) vs α_1 and β_1 when $d_{s,r} = 5$, $d_{r,1} = d_{r,2} = 2$, $\rho_S = 30dB$, $\Xi_r = -10dB$ and $\acute{R}_1 = \acute{R}_2 = 0.2$ a) R-DFNOMA b) C-DFNOMA.

the evaluations too long, we provide simulations for $\kappa_{s,r} = 0$. As expected, both power allocation coefficients (source and relay) have reverse effects on the performances of users.

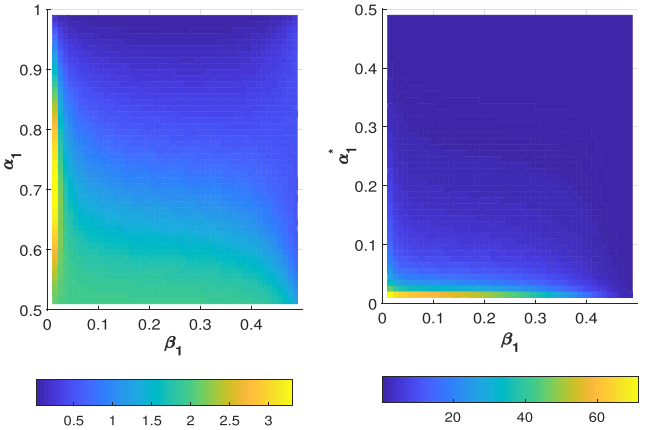

FIGURE 17. Error Fairness Index (PF_E) vs α_1 and β_1 when $d_{s,r} = 5$, $d_{r,1} = d_{r,2} = 2$ and $\rho_S = 30dB$ a) R-DFNOMA b) C-DFNOMA.

Increasing/decreasing α_1 and/or β_1 provide performance gain for one of the user and cause a decay for the other vice-versa. In terms of EC in Fig. 12, increase in α_1 and/or β_1 provide better EC for D_1 and lower EC for D_2. The same discussions are also valid for outage performances of users in Fig. 13. Nevertheless, it is noteworthy that increasing/decreasing any power allocation coefficient too much causes one of the users to be in always outage. The same performance trends can be seen for also BER in Fig. 14. However, since an actual modulation/demodulation is implemented, the effect of power allocation on the SIC performance is more clear in Fig. 14. For instance, increasing β_1 means that higher power is allocated to D_1 symbols in the second phase thereby better error performance is expected. Nevertheless, one can easily see that increasing β_1 too much causes a decay in error performance of D_1 along with error performance of D_2. This is explained as follows. Since the D_1 has to implement SIC in the second phase, increasing β_1 causes erroneous SIC more likely and this pulls down the error performance of D_1. Based on above discussions, it is clear that power allocation affects users' performances reversely (gain for one and decay for the other), thus it is not possible to define a optimum power allocation which offers the best performances for both users. Nevertheless, by considering user fairness, a sub-optimum power allocation can be obtained.

To this end, user fairness comparisons between R-DFNOMA and C-DFNOMA with respect to power allocations (α_1 and β_1) in Fig. 15 - Fig. 17 for the same conditions above comparisons. Based on user fairness for EC in Fig. 15, although PF_c changes within larger range (max. 5) in R-DFNOMA, R-DFNOMA provides better user fairness (close to 1), whereas user fairness in C-DFNOMA is close to 1.5, for most of the power allocation pairs. In Fig. 16, user fairness is presented in terms of OP when the users have same QoS requirement ($\acute{R}_1 = \acute{R}_2 = 0.2$). It can be seen that users in R-DFNOMA have similar outage performance even if power allocation coefficients change. In R-DFNOMA, one of the users may have maximum 6 times better outage performance

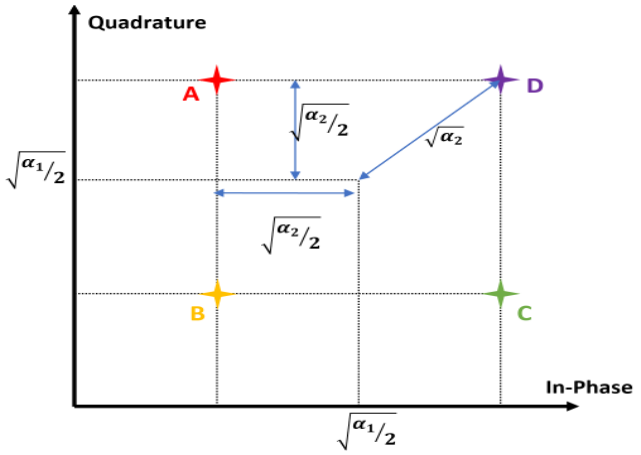

FIGURE 18. Superposition coded symbol in the first phase when $x_1 = 1/\sqrt{2} + i/\sqrt{2}$.

than the other. However, this unfairness may raise to 50 times better performance in C-DFNOMA. Lastly, user fairness in terms of error performance is presented in Fig. 17. Similar discussions can be seen for also user fairness in terms of BER from Fig. 17. The fairness index may have the maximum 3.5 in R-DFNOMA whereas the value of 80 in C-DFNOMA. This shows that users in R-DFNOMA have similar data reliability, however in C-DFNOMA, one of the users may outperform 80 times the other. Based on the results between Fig. 15 and Fig. 17, R-DFNOMA is much more robust against changes in power allocation coefficients in terms of user fairness. For the given channel conditions, by considering the user fairness in terms of all KPIs, the optimum power allocation pairs in R-DFNOMA could be defined $\alpha_1 \approx 0.85$ and $\beta_1 \approx 0.15$ where users have the same performances so that user fairness becomes very close to 1.

V. CONCLUSION

In this paper, we introduce the reversed decode-forward relaying NOMA (R-DFNOMA) to improve user fairness in conventional DFNOMA (C-DFNOMA). We consider imperfect SIC at detections and according to imperfect SIC effect and we re-define SINRs at the nodes to provide a more accurate model. Besides, we also consider imperfect CSI at the nodes. With the imperfect SIC and CSI, we investigate performance of the proposed R-DFNOMA and derive closed-form expressions for ergodic capacity (EC), outage probability (OP) and bit error probability (BEP). We also derive upper and lower bounds for EC and OP, respectively. In the BEP analysis with imperfect CSI, we prove that the effect of noise due to the imperfect CSI is quite challenging and different from the OMA schemes. The noise due to the imperfect CSI has not equal for all transmitted superposition coded symbols. For each situation, it has different variance. Then, in order to emphasize user fairness, we define fairness indexes for all KPIs (i.e., EC, OP and BEP). With the extensive simulations, derived expressions are validated and it is proved that R-DFNOMA outperforms significantly C-DFNOMA in terms of user fairness when the users have similar channel conditions. Moreover, user fairness is investigated with the change of power allocation coefficients and optimum power allocation is discussed under user fairness constraint. Based on the results and discussions, it is revealed that reversed power allocation at the source and changing SIC order at the relay can provide better user fairness and the system will be more robust against power allocation. This promising result shows that reversed networks can be implemented in other NOMA and cooperative involved systems. To this end, analysis and discussions for DF relaying in this paper can be extended for other strategies. Hence, reversed power allocation in DFNOMA with full-duplex, DFNOMA with energy harvesting and DFNOMA with direct links are seen as future research topics. Lastly, as discussed above, the BEP analysis of NOMA involved systems with imperfect CSI is another challenging issue and the analysis with imperfect CSI for all NOMA involved still waits to be resolved.

APPENDIX A
PROOF OF EQ. (37)

We write the received signal in (1) as

$$y_{s,r} = \underbrace{\sqrt{P_s}\hat{h}_{s,r}\left(\sqrt{\alpha_1}x_1 + \sqrt{\alpha_2}x_2\right)}_{\text{desired signal}} + \underbrace{\sqrt{P_s}\epsilon_{s,r}\left(\sqrt{\alpha_1}x_1 + \sqrt{\alpha_2}x_2\right)}_{\text{noise due to imperfect CSI } (\vartheta_{s,r})} + \underbrace{n_r.}_{\text{additive noise}} \quad (52)$$

Thus, if the superposition coding was not implemented -OMA systems-, the BEP would be easily defined as the probability of the total noise terms being above the desired signal amplitude. However, in NOMA, due to the superposition coding, the transmitted signals do not have equal energies. Hence, each superposition coded symbol and the imperfect CSI effect in this case should be evaluated separately since the variance of imperfect CSI noise change also according to transmitted superposition coded symbols. When both symbols are modulated by QPSK with Gray mapping, we assume that {00} bits are transmitted for the first user so the $x_1 = 1/\sqrt{2} + i/\sqrt{2}$. In this case, all possibilities (i.e., A,B,C,B) for the transmitted superposition coded symbols are represented in Fig. 18. If the received signal in (52) exceeds the decision boundaries, the erroneous detection will occur. We should consider that the imperfect CSI noise (i.e., $\vartheta_{s,r}$) in each case will have different variances [51] and they are given as $[\kappa P_s, \kappa\left(\sqrt{\alpha_1} - \sqrt{\alpha_2}\right)^2 P_s, \kappa P_s, \kappa\left(\sqrt{\alpha_1} + \sqrt{\alpha_2}\right)^2 P_s]$ for A,B,C and D. The variances of each case change according to energy of the superposition coded symbol within that case. We find the variances by considering the base-band superposition coded symbols have the energies $[1, \left(\sqrt{\alpha_1} - \sqrt{\alpha_2}\right)^2, 1, \left(\sqrt{\alpha_1} + \sqrt{\alpha_2}\right)^2]$ for A,B,C and D, respectively. This can be easily seen in Fig. 8 by the Euclidean distance for each point from that point to the origin. Without loss of generality, we consider the error probability for the *first bit* of x_1 symbols. The erroneous detection occurs

when the in phase of the received signal exceeds the in-phase boundary. In other words, when in-phase terms of the received signal becomes lower than zero, the erroneous detection will occur. This is caused by the the in-phase term of the total noise[8] (due to the imperfect CSI plus additive noise). Hence, the BEP is given by

$$P_1^I(e|_{\{00\}}) = \underbrace{\frac{1}{2}P(\Im^I + n^I < -\left(\sqrt{\alpha_1/2} - \sqrt{\alpha_2/2}\right)\sqrt{P_s}\hat{h})}_{\text{A and B situations}} + \underbrace{\frac{1}{2}P(\Im^I + n^I < -\left(\sqrt{\alpha_1/2} + \sqrt{\alpha_2/2}\right)\sqrt{P_s}\hat{h})}_{\text{C and D situations}} \tag{53}$$

where subscript $()^I$ denotes in-phase component. Considering the variances of $\Im$ in A,B,C,D, the BEP is given as

$$P_1^I(e|_{\{00\}}) = \underbrace{\frac{1}{4}Q\left(\sqrt{\frac{2\nu_1 P_s|\hat{h}|^2}{\kappa P_s + N_0}}\right)}_{A} + \underbrace{\frac{1}{4}Q\left(\sqrt{\frac{2\nu_1 P_s|\hat{h}|^2}{2\kappa\nu_1 P_s + N_0}}\right)}_{B} + \underbrace{\frac{1}{4}Q\left(\sqrt{\frac{2\nu_2 P_s|\hat{h}|^2}{\kappa P_s + N_0}}\right)}_{C} + \underbrace{\frac{1}{4}Q\left(\sqrt{\frac{2\nu_2 P_s|\hat{h}|^2}{2\kappa\nu_2 P_s + N_0}}\right)}_{D} \tag{54}$$

[8]We drop indexes for notation simplicity

where $\nu_1 = \left(\sqrt{\alpha_1/2} - \sqrt{\alpha_2/2}\right)^2$ and $\nu_2 = \left(\sqrt{\alpha_1/2} + \sqrt{\alpha_2/2}\right)^2$. Thanks to gray mapping, the BEP for the *second bit* (i.e., $P_1^Q(e|_{\{00\}})$) will be the same with (54). Hence, the average BEP $P_1(e|_{\{00\}}) = 1/2\left(P_1^I(e|_{\{00\}}) + P_1^Q(e|_{\{00\}})\right)$ is again equal to (54). Finally, thanks to the symmetry of the superposition coded symbol, the BEPs for the other cases (i.e., $\{01\}, \{10\}, \{11\}$ bits are transmitted for x_1) are obtained as in (54). Therefore, the overall BEP for x_1 is equal to (54). With some algebraic simplifications, it is derived as in (37). The proof is completed.

APPENDIX B
PROOF OF EQ. (39)

In order to obtain BEP of x_2 symbols, erroneous and correct SIC cases should be evaluated separately. Firstly, consider the correct SIC case, only x_2 symbols and noise effects (imperfect CSI and additive noises) remain after SIC. However, the same noises affect erroneous detection of x_2 symbols, thus the BEP is given by a conditional probability. Considering the imperfect CSI effects, the probabilities in [52, eq, (51)] turn out to be in (55), as shown at the bottom of this page.

In the second case, i.e., erroneous SIC, just as the previous case, the BEP is a conditional probability. Recalling imperfect CSI effect, according to [52, Table 3 and eq. (53)], the BEP is defined in (56), as shown at the bottom of this page.

The total BEP for x_2 symbols are obtained by summing two cases (i.e., correct and erroneous SIC). We firstly apply conditional probability rule in (55) and (56), and then sum them. Finally, considering the variances of each cases, as discussed

$$P_2(e|_{correct\ SIC}) = \underbrace{\frac{1}{2}\underbrace{P(\Im^I + n^I \geq -\left(\sqrt{\alpha_1/2} - \sqrt{\alpha_2/2}\right)\sqrt{P_s}\hat{h})}_{\text{correct SIC priori}} \times P(\underbrace{\Im^I + n^I < \sqrt{\alpha_2 P_s/2}\hat{h}}_{\text{error event}} | \underbrace{\Im^I + n^I \geq -\left(\sqrt{\alpha_1/2} - \sqrt{\alpha_2/2}\right)\sqrt{P_s}\hat{h}}_{\text{correct SIC condition}})}_{\text{A and B situations}} + \underbrace{\frac{1}{2}\underbrace{P(\Im^I + n^I \geq -\left(\sqrt{\alpha_1/2} + \sqrt{\alpha_2/2}\right)\sqrt{P_s}\hat{h})}_{\text{correct SIC priori}} \times P(\underbrace{\Im^I + n^I \geq -\sqrt{\alpha_2 P_s/2}\hat{h}}_{\text{error event}} | \underbrace{\Im^I + n^I \geq -\left(\sqrt{\alpha_1/2} + \sqrt{\alpha_2/2}\right)\sqrt{P_s}\hat{h})}_{\text{correct SIC condition}}}_{\text{C and D situations}} \tag{55}$$

$$P_2(e|_{error\ SIC}) = \underbrace{\frac{1}{2}\underbrace{P(\Im^I + n^I < -\left(\sqrt{\alpha_1/2} - \sqrt{\alpha_2/2}\right)\sqrt{P_s}\hat{h})}_{\text{erroneous SIC priori}} \times P(\underbrace{\Im^I + n^I \geq -\left(2\sqrt{\alpha_1/2} - \sqrt{\alpha_2/2}\right)\sqrt{P_s}\hat{h}}_{\text{error event}} | \underbrace{\Im^I + n^I < -\left(\sqrt{\alpha_1/2} - \sqrt{\alpha_2/2}\right)\sqrt{P_s}\hat{h})}_{\text{erroneous SIC condition}}}_{\text{A and B situations}} + \underbrace{\frac{1}{2}\underbrace{P(\Im^I + n^I \geq -\left(\sqrt{\alpha_1/2} + \sqrt{\alpha_2/2}\right)\sqrt{P_s}\hat{h})}_{\text{erroneous SIC priori}} \times P(\underbrace{\Im^I + n^I < -\left(2\sqrt{\alpha_1/2} + \sqrt{\alpha_2/2}\right)\sqrt{P_s}\hat{h}}_{\text{error event}} | \underbrace{\Im^I + n^I < -\left(\sqrt{\alpha_1/2} + \sqrt{\alpha_2/2}\right)\sqrt{P_s}\hat{h})}_{\text{erroneous SIC condition}}}_{\text{C and D situations}} \tag{56}$$

in the previous proof, the BEP of x_2 symbols is obtained as

$$P_2(e) = \frac{1}{4}\left[Q\left(\sqrt{\frac{2\nu_1 P_s|\hat{h}|^2}{\kappa P_s + N_0}}\right) + Q\left(\sqrt{\frac{2\nu_1 P_s|\hat{h}|^2}{2\kappa\nu_1 P_s + N_0}}\right)\right] - \frac{1}{4}\left[Q\left(\sqrt{\frac{2\nu_2 P_s|\hat{h}|^2}{\kappa P_s + N_0}}\right) + Q\left(\sqrt{\frac{2\nu_2 P_s|\hat{h}|^2}{2\kappa\nu_2 P_s + N_0}}\right)\right] + \frac{1}{4}\left[2Q\left(\sqrt{\frac{2\nu_3 P_s|\hat{h}|^2}{\kappa P_s + N_0}}\right) + Q\left(\sqrt{\frac{2\nu_3 P_s|\hat{h}|^2}{2\kappa\nu_1 P_s + N_0}}\right) + Q\left(\sqrt{\frac{2\nu_3 P_s|\hat{h}|^2}{2\kappa\nu_2 P_s + N_0}}\right)\right] - \frac{1}{4}\left[Q\left(\sqrt{\frac{2\nu_4 P_s|\hat{h}|^2}{\kappa P_s + N_0}}\right) + Q\left(\sqrt{\frac{2\nu_4 P_s|\hat{h}|^2}{2\kappa\nu_1 P_s + N_0}}\right)\right] + \frac{1}{4}\left[Q\left(\sqrt{\frac{2\nu_5 P_s|\hat{h}|^2}{\kappa P_s + N_0}}\right) + Q\left(\sqrt{\frac{2\nu_5 P_s|\hat{h}|^2}{2\kappa\nu_2 P_s + N_0}}\right)\right]. \quad (57)$$

where $\nu_3 = \frac{\alpha_2}{2}$, $\nu_4 = \left(2\sqrt{\alpha_1/2} - \sqrt{\alpha_2/2}\right)^2$ and $\nu_5 = \left(2\sqrt{\alpha_1/2} + \sqrt{\alpha_2/2}\right)^2$. With some simplifications, the BEP is derived in the form (39) so the proof is completed.

REFERENCES

[1] "Cisco visual networking index: Global mobile data traffic forecast update, 2017–2022," Cisco, San Jose, CA, USA, Tech. Rep. C11-738429-01 02/19, 2019.

[2] J. J. G. Andrews, S. Buzzi, W. Choi, S. V. S. Hanly, A. Lozano, A. A. C. K. Soong, and J. J. C. Zhang, "What will 5G be?" *IEEE J. Sel. Areas Commun.*, vol. 32, no. 6, pp. 1065–1082, Jun. 2014.

[3] M. Shirvanimoghaddam, M. Dohler, and S. J. Johnson, "Massive non-orthogonal multiple access for cellular IoT: Potentials and limitations," *IEEE Commun. Mag.*, vol. 55, no. 9, pp. 55–61, Sep. 2017.

[4] L. Dai, B. Wang, Y. Yuan, S. Han, C.-L. I, and Z. Wang, "Non-orthogonal multiple access for 5G: Solutions, challenges, opportunities, and future research trends," *IEEE Commun. Mag.*, vol. 53, no. 9, pp. 74–81, Sep. 2015.

[5] Y. Saito, Y. Kishiyama, A. Benjebbour, T. Nakamura, A. Li, and K. Higuchi, "Non-orthogonal multiple access (NOMA) for cellular future radio access," in *Proc. IEEE 77th Veh. Technol. Conf. (VTC Spring)*, Jun. 2013, pp. 1–5.

[6] Z. Ding, Z. Yang, P. Fan, and H. V. Poor, "On the performance of non-orthogonal multiple access in 5G systems with randomly deployed users," *IEEE Signal Process. Lett.*, vol. 21, no. 12, pp. 1501–1505, Dec. 2014.

[7] Z. Ding, X. Lei, G. K. Karagiannidis, R. Schober, J. Yuan, and V. K. Bhargava, "A survey on non-orthogonal multiple access for 5G networks: Research challenges and future trends," *IEEE J. Sel. Areas Commun.*, vol. 35, no. 10, pp. 2181–2195, Oct. 2017.

[8] Z. Ding, M. Peng, and H. V. Poor, "Cooperative non-orthogonal multiple access in 5G systems," *IEEE Commun. Lett.*, vol. 19, no. 8, pp. 1462–1465, Aug. 2015.

[9] F. Kara and H. Kaya, "On the error performance of cooperative-NOMA with statistical CSIT," *IEEE Commun. Lett.*, vol. 23, no. 1, pp. 128–131, Jan. 2019.

[10] J.-B. Kim and I.-H. Lee, "Capacity analysis of cooperative relaying systems using non-orthogonal multiple access," *IEEE Commun. Lett.*, vol. 19, no. 11, pp. 1949–1952, Nov. 2015.

[11] F. Kara and H. Kaya, "Error probability analysis of NOMA-based diamond relaying network," *IEEE Trans. Veh. Technol.*, vol. 69, no. 2, pp. 2280–2285, Feb. 2020.

[12] Y. Xiao, L. Hao, Z. Ma, Z. Ding, Z. Zhang, and P. Fan, "Forwarding strategy selection in dual-hop NOMA relaying systems," *IEEE Commun. Lett.*, vol. 22, no. 8, pp. 1644–1647, Aug. 2018.

[13] Y. Liu, G. Pan, H. Zhang, and M. Song, "Hybrid decode-forward & amplify-forward relaying with non-orthogonal multiple access," *IEEE Access*, vol. 4, pp. 4912–4921, 2016.

[14] Y. Liu, W. Lu, S. Shi, Q. Wu, B. Li, Z. Li, and H. Zhu, "Performance analysis of a downlink cooperative noma network over Nakagami-m fading channels," *IEEE Access*, vol. 6, pp. 53034–53043, 2018.

[15] X. Yue, Y. Liu, S. Kang, and A. Nallanathan, "Performance analysis of NOMA with fixed gain relaying over Nakagami-*m* fading channels," *IEEE Access*, vol. 5, pp. 5445–5454, 2017.

[16] X. Liang, Y. Wu, D. W. K. Ng, Y. Zuo, S. Jin, and H. Zhu, "Outage performance for cooperative NOMA transmission with an AF relay," *IEEE Commun. Lett.*, vol. 21, no. 11, pp. 2428–2431, Nov. 2017.

[17] H. Liu, Z. Ding, K. J. Kim, K. S. Kwak, and H. V. Poor, "Decode-and-forward relaying for cooperative NOMA systems with direct links," *IEEE Trans. Wireless Commun.*, vol. 17, no. 12, pp. 8077–8093, Dec. 2018.

[18] Q. Zhang, Z. Liang, Q. Li, and J. Qin, "Buffer-aided non-orthogonal multiple access relaying systems in Rayleigh fading channels," *IEEE Trans. Commun.*, vol. 65, no. 1, pp. 95–106, Jan. 2017.

[19] S. Luo and K. C. Teh, "Adaptive transmission for cooperative NOMA system with buffer-aided relaying," *IEEE Commun. Lett.*, vol. 21, no. 4, pp. 937–940, Apr. 2017.

[20] D. Wan, M. Wen, F. Ji, Y. Liu, and Y. Huang, "Cooperative NOMA systems with partial channel state information over Nakagami-*m* fading channels," *IEEE Trans. Commun.*, vol. 66, no. 3, pp. 947–958, Mar. 2018.

[21] J. Men, J. Ge, and C. Zhang, "Performance analysis for downlink relaying aided non-orthogonal multiple access networks with imperfect CSI over Nakagami-*m* fading," *IEEE Access*, vol. 5, pp. 998–1004, 2017.

[22] X. Li, J. Li, and L. Li, "Performance analysis of impaired SWIPT NOMA relaying networks over imperfect weibull channels," *IEEE Syst. J.*, vol. 14, no. 1, pp. 669–672, Mar. 2020.

[23] X. Li, J. Li, Y. Liu, Z. Ding, and A. Nallanathan, "Residual transceiver hardware impairments on cooperative NOMA networks," *IEEE Trans. Wireless Commun.*, vol. 19, no. 1, pp. 680–695, Jan. 2020.

[24] X. Li, M. Liu, C. Deng, P. T. Mathiopoulos, Z. Ding, and Y. Liu, "Full-duplex cooperative NOMA relaying systems with I/Q imbalance and imperfect SIC," *IEEE Wireless Commun. Lett.*, vol. 9, no. 1, pp. 17–20, Jan. 2020.

[25] Z. Ding, H. Dai, and H. Vincent Poor, "Relay selection for cooperative NOMA," *IEEE Wireless Commun. Lett.*, vol. 5, no. 4, pp. 416–419, Aug. 2016.

[26] Z. Yang, Z. Ding, Y. Wu, and P. Fan, "Novel relay selection strategies for cooperative noma," *IEEE Trans. Veh. Technol.*, vol. 66, no. 11, pp. 10114–10123, Nov. 2017.

[27] P. Xu, Z. Yang, Z. Ding, and Z. Zhang, "Optimal relay selection schemes for cooperative NOMA," *IEEE Trans. Veh. Technol.*, vol. 67, no. 8, pp. 7851–7855, Aug. 2018.

[28] D. Deng, L. Fan, X. Lei, W. Tan, and D. Xie, "Joint user and relay selection for cooperative noma networks," *IEEE Access*, vol. 5, pp. 20220–20227, 2017.

[29] Y. Xu, H. Sun, R. Q. Hu, and Y. Qian, "Cooperative non-orthogonal multiple access in heterogeneous networks," in *Proc. IEEE Global Commun. Conf. (GLOBECOM)*, Dec. 2015, pp. 1–6.

[30] M. F. Kader, M. B. Shahab, and S. Y. Shin, "Exploiting non-orthogonal multiple access in cooperative relay sharing," *IEEE Commun. Lett.*, vol. 21, no. 5, pp. 1159–1162, May 2017.

[31] M. F. Kader, S. Y. Shin, and V. C. M. Leung, "Full-duplex non-orthogonal multiple access in cooperative relay sharing for 5G systems," *IEEE Trans. Veh. Technol.*, vol. 67, no. 7, pp. 5831–5840, Jul. 2018.

[32] X. Yue, Y. Liu, S. Kang, A. Nallanathan, and Y. Chen, "Modeling and analysis of two-way relay non-orthogonal multiple access systems," *IEEE Trans. Commun.*, vol. 66, no. 9, pp. 3784–3796, Sep. 2018.

[33] G. Im and J. H. Lee, "Outage probability for cooperative NOMA systems with imperfect SIC in cognitive radio networks," *IEEE Commun. Lett.*, vol. 23, no. 4, pp. 692–695, Apr. 2019.

[34] F. Kara and H. Kaya, "BER performances of downlink and uplink NOMA in the presence of SIC errors over fading channels," *IET Commun.*, vol. 12, no. 15, pp. 1834–1844, Sep. 2018.

[35] T. Assaf, A. Al-Dweik, M. E. Moursi, and H. Zeineldin, "Exact BER performance analysis for downlink NOMA systems over Nakagami-*m* fading channels," *IEEE Access*, vol. 7, pp. 134539–134555, 2019.

[36] S. Timotheou and I. Krikidis, "Fairness for non-orthogonal multiple access in 5G systems," *IEEE Signal Process. Lett.*, vol. 22, no. 10, pp. 1647–1651, Oct. 2015.

[37] F. Liu, P. Mahonen, and M. Petrova, "Proportional fairness-based user pairing and power allocation for non-orthogonal multiple access," in *Proc. IEEE 26th Annu. Int. Symp. Pers., Indoor, Mobile Radio Commun. (PIMRC)*, Aug. 2015, pp. 1127–1131.
[38] Y. Liu, M. Elkashlan, Z. Ding, and G. K. Karagiannidis, "Fairness of user clustering in MIMO non-orthogonal multiple access systems," *IEEE Commun. Lett.*, vol. 20, no. 7, pp. 1465–1468, Jul. 2016.
[39] F. Liu, P. Mahonen, and M. Petrova, "Proportional fairness-based power allocation and user set selection for downlink NOMA systems," in *Proc. IEEE Int. Conf. Commun. (ICC)*, May 2016, pp. 1–6.
[40] F. Kara and H. Kaya, "The error performance analysis of the decode-forward relay-aided-NOMA systems and a power allocation scheme for user fairness," *J. Fac. Eng. Archit. Gazi Univ.*, vol. 35, no. 1, pp. 97–108, 2020.
[41] F. Kara and H. Kaya, "Error analysis of decode-forward cooperative relaying NOMA schemes over Nakagami-*m* fading channels," in *Proc. 28th Signal Process. Commun. Appl. Conf.*, Gaziantep, Turkey, 2020, pp. 1–4.
[42] *Downlink Multiuser Superposition Transmission for LTE*, document RP-160680, 3GPP, 2016.
[43] X. Li, M. Huang, C. Zhang, D. Deng, K. M. Rabie, Y. Ding, and J. Du, "Security and reliability performance analysis of cooperative multi-relay systems with nonlinear energy harvesters and hardware impairments," *IEEE Access*, vol. 7, pp. 102644–102661, 2019.
[44] S. Ross, *A First Course in Probability*, vol. 56, no. 3. Upper Saddle River, NJ, USA: Prentice-Hall, 1988.
[45] I. Gradshteyn and I. Ryzhik, *Table of Integrals, Series, and Products*, 5th ed. San Diego, CA, USA: Academic, Feb. 1994.
[46] I.-H. Lee and J.-B. Kim, "Average symbol error rate analysis for non-orthogonal multiple access with *M* -Ary QAM signals in Rayleigh fading channels," *IEEE Commun. Lett.*, vol. 23, no. 8, pp. 1328–1331, Aug. 2019.
[47] F. Kara and H. Kaya, "Threshold-based selective cooperative-NOMA," *IEEE Commun. Lett.*, vol. 23, no. 7, pp. 1263–1266, Jul. 2019.
[48] M.-S. Alouini and A. J. Goldsmith, "A unified approach for calculating error rates of linearly modulated signals over generalized fading channels," *IEEE Trans. Commun.*, vol. 47, no. 9, pp. 1324–1334, 1999.
[49] Z. Ding, Z. Zhao, M. Peng, and H. V. Poor, "On the spectral efficiency and security enhancements of NOMA assisted multicast-unicast streaming," *IEEE Trans. Commun.*, vol. 65, no. 7, pp. 3151–3163, Jul. 2017.
[50] M. Vaezi, R. Schober, Z. Ding, and H. V. Poor, "Non-orthogonal multiple access: Common myths and critical questions," *IEEE Wireless Commun.*, vol. 26, no. 5, pp. 174–180, Oct. 2019.
[51] F. Kara and H. Kaya, "Error probability analysis of non-orthogonal multiple access with channel estimation errors," in *Proc. IEEE Int. Black Sea Conf. Commun. Netw.*, Odyssey, Ukraine, 2020, pp. 1–5.
[52] F. Kara and H. Kaya, "Performance analysis of SSK-NOMA," *IEEE Trans. Veh. Technol.*, vol. 68, no. 7, pp. 6231–6242, Jul. 2019.

FERDI KARA (Member, IEEE) received the B.Sc. degree (Hons.) in electronics and communication engineering from Suleyman Demirel University, Turkey, in 2011, and the M.Sc. and Ph.D. degrees in electrical and electronics engineering from Zonguldak Bülent Ecevit University, Turkey, in 2015 and 2019, respectively. Since 2011, he has been working with the Wireless Communication Technologies Research Laboratory (WCTLab), Zonguldak Bülent Ecevit University, where he is currently a Senior Researcher. His research interests include wireless communications specified with NOMA, MIMO systems, cooperative communication, index modulations, energy harvesting, and machine learning in physical communication. He was awarded the Exemplary Reviewer Certificate for the IEEE COMMUNICATIONS LETTERS, in 2019. He serves as a regular Reviewer for reputed IEEE journals and conferences.

HAKAN KAYA received the B.Sc., M.Sc., and Ph.D. degrees from Zonguldak Karaelmas University, Turkey, in 2007, 2010, and 2015, respectively, all in electrical and electronics engineering. Since 2015, he has been working as an Assistant Professor with Zonguldak Bülent Ecevit University and the Head of the Wireless Communication Technologies Research Laboratory (WCTLab). His research interests include cooperative communication, NOMA, turbo coding, and machine learning.